2011

Iron and manganese reduction in Bering Sea shelf sediments

Margaret E.S. Esch
Western Washington University

IRON AND MANGANESE REDUCTION IN BERING SEA SHELF SEDIMENTS

By

Margaret E.S. Esch

Accepted in Partial Completion
Of the Requirements for the Degree
Master of Science

Moheb A. Ghali, Dean of the Graduate School

ADVISORY COMMITTEE

Chair, Dr. David H. Shull

Dr. Allan H. Devol

Dr. John M. Rybczyk

MASTER'S THESIS

In presenting this thesis in partial fulfillment of the requirements for a master's degree at Western Washington University, I grant to Western Washington University the on-exclusive royalty-free right to archive, reproduce, distribute, and display the thesis in any and all forms, including electronic format, via any digital library mechanisms maintained by WWU.

I represent and warrant this is my original work, and does not infringe or violate any rights of others. I warrant that I have obtained written permissions from the owner of any third party copyrighted material included in these files.

I acknowledge that I retain ownership rights to the copyright of this work, including but not limited to the right to use all or part of this work in future works, such as articles or books.

Library users are granted permission for individual, research and non-commercial reproduction of this work for educational purposes only. Any further digital posting of this document requires specific permission from the author.

Any copying or publication of this thesis for commercial purposes, or for financial gain, is not allowed without my written permission.

Margaret Esch
May 4, 2011

IRON AND MANGANESE REDUCTION IN BERING SEA SHELF SEDIMENTS

A Thesis

Presented to

The Faculty of

Western Washington University

In Partial Fulfillment

Of the Requirements for the Degree

Master of Science

By

Margaret E.S. Esch

February 2011

Abstract

The southeastern Bering Sea is known for high levels of primary productivity, which is iron-limited in off-shore waters. The sedimentary reduction of iron and manganese oxides can be significant pathways of organic matter oxidation in marine sediments, and may influence patterns of primary production in surface waters. The goal of this research was to investigate patterns of Fe and Mn reduction rates across the shelf of the southeastern Bering Sea, and to assess the relative importance of these pathways in sedimentary organic matter remineralization. During the spring and summer of 2009, sediment samples were collected from 36 locations across the Bering shelf. At each sampling location, sediment oxygen consumption was directly measured using incubation cores, which were then used to estimate rates of total organic carbon oxidation. Bioturbation rates were quantified using profiles of excess ^{234}Th, and depth profiles of solid-phase iron and manganese oxide concentrations were generated for each station sampled. These were then used to calculate the relative rates of both iron and manganese oxide reduction. Results varied across the Bering shelf. Average rates of bioturbation were highest in the northern region (mean: 6.29 $cm^2\ yr^{-1}$), and lowest in the off-shelf region (mean: 1.37 $cm^2\ yr^{-1}$). Rates of Fe oxide reduction, as well as the percentage of carbon oxidized by iron reduction, followed the same trend. The average rate of Fe reduction across the shelf was approximately 1.74 mmole $m^{-2}\ d^{-1}$; however, rates greater than 6 mmole $m^{-2}\ d^{-1}$ were calculated in the northern region. Conversely, Mn oxide reduction was found to be of minor significance, with low reduction rates in all regions, averaging only 0.09 mmole $m^{-2}\ d^{-1}$ across the shelf, and accounting for no more than 5% of total carbon oxidation in any region. These results indicate that Fe oxide reduction is a

significant pathway for carbon remineralization in the northern and middle-shelf regions, where organic matter deposition rates and benthic biomass are high. Additionally, this work provides insight into the potential role of sedimentary iron reduction in providing bioavailable Fe for phytoplankton communities in this region.

Acknowledgements

Several people contributed to the completion of this thesis, and it is my pleasure to take this opportunity to express my sincere gratitude.

First, none of this would have been possible without the captain and crew of both the USCGC Healy and the R/V Knorr. During my time at sea, Heather Whitney was a great help with sample collection and processing, and Pat Kelly provided much assistance with radioisotope analysis.

Back on land, Erin Macri and Clint Burgess graciously assisted with sample analysis and numerous instrumentation repairs, enabling me to finish in a timely manner. The time they gave is very much appreciated.

I would like to thank my committee member, John Rybczyk, for his helpful comments. I hope this thesis provides many entertaining fireside readings. Also on my committee, Allan Devol provided valuable insights and great shipboard company. I'm glad I had a chance to go to sea with you.

I would never have discovered my love for the mud, were it not for my advisor, David Shull. Always enthusiastic and never missing an opportunity to teach, I have learned so much from him. His thoughtful and sound advice regarding not only my research, but science and life in general will not be forgotten. Thank you for being such a wonderful mentor.

Last, but certainly not least, I am wholly indebted to my parents for their unwavering support throughout this process and all of my endeavors. So much of what I have accomplished I owe to you, and I hope you know how grateful I am for the both of you.

This research was funded by the National Science Foundation (ARC0612380 and MRI0723234 to David Shull) as part of the Bering Ecosystem Study.

Table of Contents

List of Tables

List of Figures

1.0 Introduction

Coastal and shelf sediments play an important role in the remineralization of organic matter (OM) and subsequent return of nutrients to the water column, supporting primary production in surface waters. The rates and pathways of OM remineralization in sediments can be complex and difficult to quantify, and much effort has been made to understand these processes in many marine benthic environments (e.g.: Canfield et al. 1993a, Thamdrup and Canfield 1996, Wang and Van Cappellen 1996, Giblin et al. 1997, Marinelli et al. 1998, Jensen et al. 2003). Iron (Fe) and manganese (Mn) oxide reduction, in particular, are major pathways for carbon oxidation is some marine sediments (Aller 1990, Canfield et al. 1993b, Aller 1994b, Thamdrup et al. 2000, Wijsman et al. 2001), including arctic regions (Glud et al. 2000, Kostka et al. 2002, Berg et al. 2003, Vandieken et al. 2006, Nickel et al. 2008). The flux of reduced Fe and Mn from the sediment as a result of the reduction of their oxides may be a significant source of Fe and Mn to surface waters, with Fe having a considerable influence on primary production (Bruland and Lohan 2003, Hurst et al. 2010). For instance, it's been estimated that Fe is a limiting nutrient for phytoplankton growth in 40% of the world's oceans (Moore et al. 2002). The study of Fe and Mn oxide reduction in marine sediments will allow for a greater understanding of their contribution to OM remineralization, as well as their role in important marine processes such as carbon preservation, nutrient regeneration and primary production.

The remineralization of carbon in marine sediments involves a number of oxidative pathways utilizing different terminal electron acceptors (Fig. 1, Table 1). Respiration through each of these pathways and their location in the sediment is governed

by their free energy yield per mole of carbon oxidized, with oxygen as the highest free energy yielding oxidant. Once oxygen becomes depleted, respiration continues via the next most efficient terminal electron acceptor. The predicted sequence of pathways is as follows: oxygen, followed by nitrate, then manganese (Mn) and iron (Fe) oxides, and sulfate (Fig.1; Froelich et al. 1979, Burdige 1993, 2006).

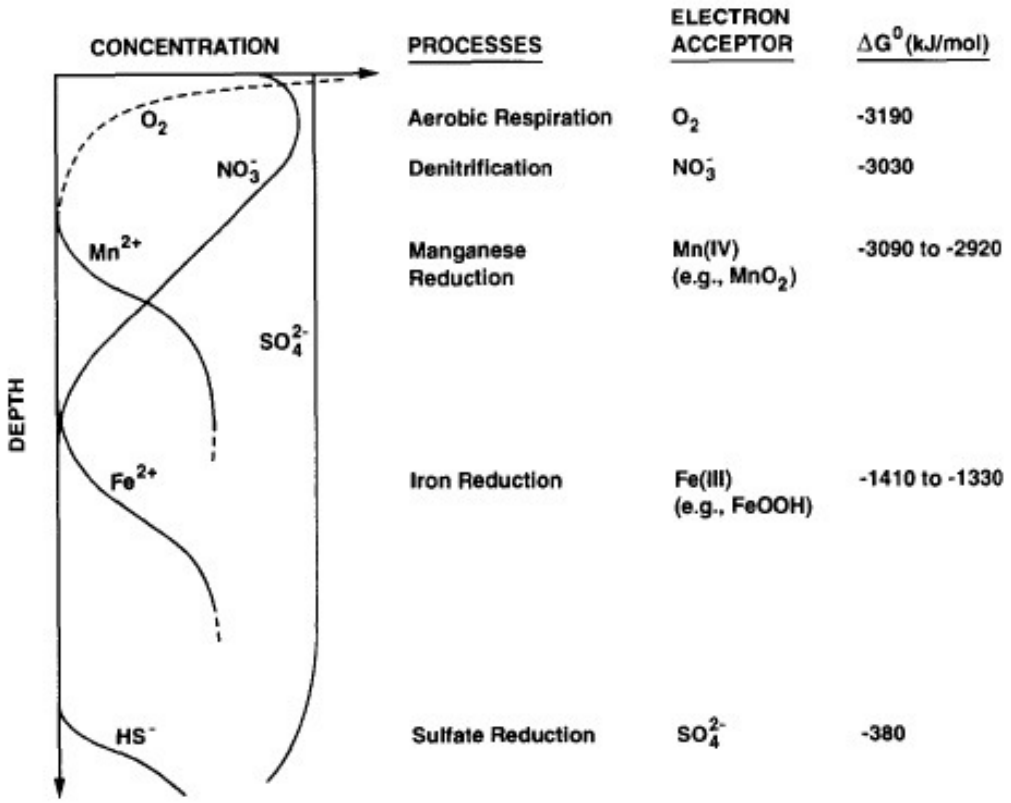

Figure 1. A simple model of the predicted sequence of respiratory pathways in marine sediments based on the free energy yield (ΔG) of each electron acceptor. The predicted pore-water profiles for each oxidant is shown at the left. (Borrowed from Burdige 1993.)

Table 1. Generalized reactions for the remineralization of OM in marine sediments, utilizing different electron acceptors. C_{org} refers to organic carbon of the formula: $(CH_2O)_{106}(NH_3)_{16}(H_3PO_4)$, from Froelich et al. (1979).

Electron acceptor	Equation for oxidation of organic carbon (C_{org})
Oxygen	$C_{org} + 138\ O_2 \rightarrow 106\ CO_2 + 16\ HNO_3 + H_3PO_4 + 122\ H_2O$
Nitrate	$C_{org} + 94.4\ HNO_3 \rightarrow 106\ CO_2 + 55.2\ N_2 + H_3PO_4 + 177.2\ H_2O$
Manganese	$C_{org} + 236\ MnO_2 + 472H^+ \rightarrow 236\ Mn^2 + 106\ CO_2 + 8\ N_2 + H_3PO_4 + 366\ H_2O$
Iron	$C_{org} + 424\ FeOOH + 848\ H^+ \rightarrow 424\ Fe^{2+} + 106\ CO_2 + 16\ NH_3 + H_3PO_4 + 742\ H_2O$
Sulfate	$C_{org} + 53\ SO_4^{2-} \rightarrow 106CO_2 + 16NH_3 + 53\ S^{2-} + H_3PO_4 + 106\ H_2O$

The depth of the oxic zone varies with OM oxidation rates and particle and pore-water transport. At low rates of OM oxidation, as is typically observed in deep-sea, pelagic sediments, aerobic respiration is usually sufficient to remineralize most of the OM (Burdige 2006, Emerson and Hedges 2003). But as OM input to the sediment and OM oxidation rates increase, the aerobic zone becomes shallower as result of the increased rate of oxygen consumption. The depletion of pore-water oxygen before the complete remineralization of available OM allows anaerobic respiration pathways to become more significant (Martin and Sayles 2003).

Iron and Mn oxide reduction can be significant not only in the remineralization of OM, but also in the redox cycles of other terminal electron acceptors (Burdige 1993). The relative importance of Fe and Mn oxide reduction in marine sediments varies, but both have been found to be important pathways for carbon oxidation in numerous studies (Aller 1994b, Glud et al. 2000, Thamdrup et al. 2000, Wijsman et al. 2001, Kostka et al. 2002, Vandieken et al. 2006, Nickel et al. 2008). Aller (1990) found Mn oxide reduction to account for approximately 100 percent of carbon oxidation in sediments of the Panama Basin. However, the reduction of Fe and Mn oxides are often indirectly linked to the remineralization of OM via the redox cycling of other electron acceptors. For instance,

the reduction of Mn oxides has been found to be coupled to anoxic nitrification (Hulth et al. 1999), as well as the oxidation of reduced Fe (Lovley 1991, Burdige 1993). Sulfide, an end product of sulfate reduction, has also been found to react with Fe or Mn oxides or reduced Fe to form elemental sulfur or Fe sulfides (Lovley 1991, Burdige 2006). Thus, Fe and Mn in sediments can also be significant as intermediate electron acceptors, indirectly coupled to OM remineralization.

Although higher OM deposition rates should correlate with higher OM oxidation rates and a greater significance of anaerobic remineralization pathways, the relative contribution of Fe and Mn oxide reduction relies on their initial availability in sediments. For example, Vandieken et al. (2006) found Mn oxide reduction to be of minor importance due to low Mn oxide concentrations and shallow depth distribution in Barents Sea sediments. In addition to high concentrations of Fe and Mn oxides, their regeneration and transport are also important factors in allowing for the sustained cycling and reduction of these metal oxides (Aller 1990, Canfield et al. 1993a, Aller 1994b). Both Fe and Mn oxides are unique electron acceptors in that they are insoluble in their oxidized form, necessitating a mechanism other than molecular diffusion for their transport within the sediment. The most important mechanism for transporting solids within surficial sediments is bioturbation.

Bioturbation can be defined as the mixing and movement of sediment particles as a result of faunal activity (Richter 1952), and it provides the means by which Fe and Mn oxides are transported in the sediment. Bioturbation not only delivers Fe and Mn oxides to reducing layers of the sediment, but can also be significant in the upward transport of reduced Fe and Mn buried or sequestered as sulfide compounds, further enhancing the

cycling of these trace metals (Burdige 2006). Pore-water irrigation also plays a role in sedimentary Fe and Mn cycling, enhancing the flux of reduced Fe and Mn to oxidizing layers of the sediment, promoting either their oxidation and further cycling, or in some cases, a loss of reduced Fe and Mn to the water column (Aller 1994a, b). Additionally, reduced Fe can often be particulate (Thamdrup 2000), and both soluble Fe and Mn can adsorb onto sediment particles containing their own oxidized forms, requiring reduced phases of Fe and Mn to be transported via particle mixing as well (Canfield et al. 1993b).

The patterns of Fe and Mn oxide reduction, as well as their relative importance in OM remineralization in the shelf sediments of the southeastern Bering Sea was the primary focus of this research. The various regions of the southeastern Bering Sea shelf provide a range of environmental conditions under which these remineralization pathways can be studied, which may provide insight into the environmental factors that influence Fe and Mn reduction in sediments. This, along with the ecological significance of this region and economic importance for fisheries, makes it an ideal study site.

1.1 Study Site

The southeastern Bering Sea shelf is broad (> 500 km) and makes up approximately half of the total area of the Bering Sea, with the rest consisting of a deep basin, referred to here as the off-shelf region (Hood 1981). The shelf waters north of 61° latitude will be referred to as the northern region. South of 61° latitude the shelf waters can be separated into three regions during ice-free conditions; the coastal (0-50 m), middle (50-100 m) and outer-shelf (100-200 m) regions. Distinct oceanographic fronts separate each of these shelf regions. The inner front separates the coastal and middle

regions, the outer front separates the middle and outer regions and the shelf-break separates the outer region from the off-shelf waters (Stabeno et al. 2001, Hunt et al. 2002, Figs. 2 & 3). These fronts greatly reduce cross-shelf advection of nutrient-rich waters during the summer months, significantly impacting primary production and ecosystem structure. For instance, surface waters in the middle-shelf region usually become depleted of nutrients by early summer, but the fronts bordering this region prevent the loss of nutrient-rich bottom water which can be transported to the surface supporting primary production later in the summer (Stabeno and Hunt 2002). Furthermore, weakened cross-shelf circulation between the middle and outer-shelf regions due to the outer front can constrain zooplankton biomass to the outer region, lowering grazing in the middle region, and allowing for more organic matter to fall to the benthos, compared to the outer region (Walsh and McRoy 1986, Coyle et al. 2007). Additionally, high rates of primary production have been observed in the northern region (Cooper et al. 2002), and Grebmeier et al. (1988) found that high quality, nitrogen-rich OM reaches the sediment surface in this region, possibly supporting the high benthic standing stocks found here. The relationship among water column production, OM supply to the sediment surface and benthic processes, referred to as benthic-pelagic coupling, is generally expected to be strong in the relatively shallow northern region of the Bering Sea (Grebmeier et al. 1989).

Strong, or efficient benthic-pelagic coupling, characterized by high rates of primary production in the water column, and reduced grazing by zooplankton, results in a high flux of OM to the sediment surface (Lovvorn et al. 2005, Grebmeier et al. 2006), which may contribute to the reasonably high rates of sedimentary carbon remineralization that is characteristic of the northern region (Grebmeier et al. 1989). Likewise, Walsh and

McRoy (1986) estimated that more than half of the spring primary production is exported to the benthos in the middle and outer-shelf regions as well; however, the percentage was much greater in the middle shelf, compared to the outer-shelf region. Thus, there is regional variation in OM supply to the sediment, and benthic-pelagic coupling efficiency across the Bering shelf. Since water depth and zooplankton grazing rates increase from the northern region toward the shelf-break, I expect that carbon exported to the benthos likely decreases across the shelf, with export highest in the northern region, followed by the middle shelf, then the outer shelf and finally the off-shelf region. Furthermore, a regional variation in OM supply to the sediment will likely lead to variation in rates and pathways of sedimentary OM remineralization as well.

The shelf region of the Bering Sea is productive, having nitrate-limited, Fe-replete surface waters. In contrast, the off-shelf region has been described as an Fe-limited, high-nutrient low-chlorophyll regime (Aguilar-Islas et al. 2007, Hurst et al. 2010). Hurst et al. (2010) suggested that Fe oxide reduction in sediments may be a significant source of bioavailable Fe to surface waters in the shelf region. Thus, OM degradation pathways in Bering shelf sediments and, in particular, the processes controlling Fe and Mn reduction might ultimately control the supply of bioavailable iron to primary producers. A possible shift in energy flow from the benthic to the pelagic ecosystem in this region due to changing climate patterns (Hunt et al. 2002, Grebmeier et al. 2006) could have a significant impact on sedimentary OM remineralization rates, and therefore the overall productivity of the Bering Sea.

1.2 Hypotheses

If greater OM export to the benthos results in increased rates of sediment oxygen consumption (Grebmeier et al. 2006), then rapid depletion of pore-water oxygen should result in increased importance of anaerobic remineralization pathways (Martin and Sayles 2003). I hypothesize that Fe and Mn reduction rates will be higher and account for a greater percentage of organic carbon oxidation in regions with higher carbon export to the benthos and thus more efficient benthic-pelagic coupling. Furthermore, if high benthic biomass is another characteristic of regions with higher OM supply (Grebmeier et al. 1988), then higher rates of bioturbation could lead to the enhanced cycling of Fe and Mn oxides in the sediment, again increasing the potential for Fe and Mn oxide reduction. Therefore, based on the expected regional variation in OM supply to the sediment, I hypothesize that Fe and Mn reduction rates will follow the same regional pattern. That is, rates will be highest in the northern region, followed by the middle shelf, then the outer shelf and lowest in the off-shelf region.

Using rates of sediment oxygen consumption as an indicator of OM supply to the benthos (Grebmeier et al. 2006), I can test this hypothesis by comparing measured rates of oxygen flux to Fe or Mn reduction rates. Therefore, I also hypothesize that Fe and Mn reduction rates will positively covary with rates of sediment oxygen consumption.

2.0 Sampling and Methods

Samples were collected over the course of two research cruises during the spring of 2009 (April 1-May 13), aboard the USCGC Healy (HLY0902), and during the summer of the same year (June 12- July 13), aboard the R/V Knorr (KN195-10). Twenty stations were sampled in spring and nineteen stations were sampled during the summer cruise (Table 2, Figs. 2 and 3). Up to 16 sample cores 10 cm in diameter and up to 40 cm in length were collected at each site using an Oceans Instruments MC-800 multicore.

2.1 Shipboard Analyses

a. Thorium-234

Particle-reactive ^{234}Th, with a half-life of 24.1 days, is an appropriate tracer for determining bioturbation rates in surficial sediments (Aller and Cochran 1976). At each station one core was selected for ^{234}Th analysis, and was sectioned in 0.5-cm increments to 2 cm and 1-cm increments to 5 cm. Each section was placed into a 125-ml polypropylene jar and dried for approximately 24 h at approximately 70 °C. After the sediment was dried, approximately 15 ml was ground and placed into a clean 125-ml jar. Total ^{234}Th activity was measured on a high-purity germanium gamma spectrometer (Canberra GL2820R), at the 63.3 keV energy peak. The first three depths of each station were counted aboard the ship until the counting error reduced to 10%, or approximately 24 h. Remaining depths were counted on shore at the end of the cruise. Counts were corrected for background, and detector efficiencies were determined by counting a standard created by adding reference-grade 0.05% Uranium pitchblende (U.S. Dept. of Energy) to sediment from the study site.

At least five months after the initial total ^{234}Th counts, the samples were recounted to determine supported activity. These values were subtracted from the total ^{234}Th activities to determine excess ^{234}Th activity (dpm g^{-1}). The resulting profile was used to determine bioturbation rates using the following equation:

$$\frac{\partial A}{\partial t} = D_b \frac{\partial^2 A}{\partial z^2} - \lambda A \qquad (1)$$

Where: A = excess ^{234}Th activity (dpm g^{-1} dry weight)

D_b = bioturbation or particle mixing rate (cm^2 yr^{-1})

λ = the first-order radioactive decay coefficient for ^{234}Th (10.5 yr^{-1}).

Assuming steady-state conditions and constant porosity and with the boundary conditions of $A = A_0$ at $z = 0$ and $A = 0$ at $z = \infty$, the solution is:

$$A = A_0 e^{\sqrt{\frac{\lambda}{D_b}} z} \qquad (2)$$

Rates of bioturbation were then estimated from the slope of the linear regression of $\ln(A)$ versus depth.

b. Whole Core Incubations

Up to three cores per station were incubated for the determination of oxygen consumption rates. These were subcored using polyethylene tubes 8 cm in diameter. The cores were stored in the dark at near *in situ* temperature (2°C), uncapped, for approximately 24 hours, after which they were sealed with silicone stoppers equipped with magnetic stirrers. Pre-inserted into each silicone stopper were two lengths of nylon tubing, fitted with two-way valves. One length of tubing was connected to a reservoir of

bottom water collected during the time of sampling. This reservoir allowed for samples of overlying water to be collected without the introduction of air bubbles. The cores were incubated for a period of 2-5 days during which a time series of samples from the overlying water were taken. One sample was taken at each time point and immediately used for the measurement of oxygen concentrations, using an optode optical microsensor (PreSens Microx TX3), calibrated before and after each reading. A 32 ppm salt solution equilibrated with the atmosphere and kept at *in situ* temperature was used for 100% saturation of oxygen, and a solution of sodium sulfite in seawater was used to zero the optode. Oxygen fluxes were then determined using:

$$J = \left.\frac{dC}{dt}\right|_{t=0} VA^{-1} \qquad (3)$$

Where: J = flux (of oxygen, Fe, etc) in μmole m^{-2} d^{-1}

$\left.\frac{dC}{dt}\right|_{t=0}$ = initial change in concentration

V = the volume of overlying water

A = the area of the incubation core

Oxygen fluxes were later corrected, using an empirical formula (*y=1.125x+3.365*, where *y* = corrected flux and *x* = uncorrected flux), for a small rate of diffusion through the silicone stoppers used during incubations.

c. Pore-water Oxygen Penetration Depth

At each station, vertical oxygen pore-water profiles were also taken, on a separate core, using a Unisense Clark-type microelectrode (Revsbech 1989). These profiles were used

to determine the depth at which pore-water oxygen concentrations reached zero. Through the use of a micromanipulator, the probe was lowered into the sediment in 0.5-mm intervals. A two-point calibration was used to convert pico amperes to dissolved oxygen concentrations. A 32 ppm salt solution equilibrated with the atmosphere and kept at *in situ* temperature was used for 100% saturation of oxygen, whereas the zero oxygen reading was determined from the bottom of the dissolved oxygen profile.

d. Pore-water profiles of Nitrate, Iron and Manganese

At each station, two cores were collected for porosity and vertical pore-water profiles. These cores were sectioned at the following depths: 0-0.5, 0.5-1, 1-1.5, 1.5-2, 2-3, 3-4, 5-6, 7-8, 9-10, 12-14, 14-16, and 19-20 cm. Approximately 3 ml of sediment from each depth was saved and frozen in a 12x75 mm tube for porosity measurements. Remaining sediment from each depth was packed into centrifuge tubes and centrifuged at 10,000 rpm for 20 minutes to separate the pore-water from the solid phase. After centrifugation, the pore-water was decanted into a 10 ml Luer-lok™ syringe and filtered through a 0.45-μm filter into a 20 ml high-density, polyethylene scintillation vial. Filtration was completed under a nitrogen-gas atmosphere in a glove bag. Pore-water nitrate analysis was completed as described by Gordon et al. (1994) on a Smartchem discrete autoanalyzer (Westco Scientific), with cadmium reduction to nitrite. After the completion of nutrient analyses, any remaining sample was frozen for Fe and Mn analysis in the lab.

e. Benthic fauna

Benthic faunal samples were collected from two cores at each station. Sediment from each core was wet-sieved using seawater through 500-μm mesh. Retained organisms were fixed in a 10% buffered formalin solution and stored until the end of the cruise. Samples were later transferred to a 70% ethanol solution and stained with Rose Bengal. Through the use of a dissecting scope, each sample was sorted; organisms were identified to major taxa, and then enumerated.

2.2 Laboratory Analyses

a. Porosity

Sediment collected for porosity measurements was stored frozen until analysis. Samples were then thawed, weighed wet, dried at 65° C for 48 hours, and then reweighed. Sediment porosity was then calculated using:

$$Porostiy = \frac{wetweight - dryweight}{(wetweight - dryweight)/(dryweight/\rho)} \quad , \qquad (4)$$

where ρ = density of particles (2.65 g cm^{-3}). Porosities were corrected for pore-water salt content.

b. Solid-phase Iron and Manganese

Sediment samples for solid-phase iron and manganese analysis were taken from the same core as pore-water samples. This core was sectioned in 0.5-cm increments to 2 cm and then in 1-cm increments to 10 cm. Subsamples of sediment from each depth were placed

into 20-ml high-density polyethylene scintillation vials. Samples were stored frozen and then freeze-dried and powdered using a mortar and pestle.

Iron and manganese oxides were extracted from freeze-dried sediment with acidified ammonium-oxalate (AAO). This extraction method has been shown to dissolve Fe oxyhydroxides without attacking silicates or crystalline goethite (Robbins et al. 1984). This method was also used for the analysis of Mn oxides. Briefly, 25 ml of 0.2M ammonium oxalate/0.1M oxalic acid solution (pH=3) was added to 0.1 g ground, freeze-dried sediment in a 50 ml centrifuge tube. These were extracted for four hours, in the dark, on a shaker table, and then centrifuged for 15 minutes at 7000 rpm. Each sample was then diluted to 50 ml and filtered through a 0.45μm filter into a low-density polyethylene bottle and stored in the refrigerator until analysis (Phillips and Lovely 1987, Davenport 2008). Concentrations of Fe and Mn oxides were determined using flame absorption spectrophotometry (Varian SpectrAA 220FS). Standards (Fisher Scientific, 1000 ppm Fe/Mn in 1.5% nitric acid) and blanks were run with each set of samples, and a continuing calibration verification and continuing calibration blank were run every 12 samples.

Since Fe and Mn oxides exist naturally as components of the sediment-particle matrix, but are also deposited to the sediment surface through sorption onto sinking particles or from precipitation of dissolved species, I used excess concentrations of Fe and Mn oxides in the sediment, which represent the exchangeable portion of these elements, to calculate Fe and Mn reduction rates. Excess concentrations are defined here as the concentrations of Fe or Mn greater than the minimum concentration first reached with depth in each vertical profile (Aller 1994b).

In order to calculate Fe and Mn reduction rates, a polynomial (2-4 order) was fit to each profile of excess solid-phase Fe and Mn. Then, assuming steady-state conditions and a constant mixing rate, the rate of Fe or Mn oxide reduction was calculated using the following relation:

$$\Sigma R_{(z)} = D_b \frac{\partial^2 C}{\partial z^2} \quad (5)$$

Where: C = excess concentrations of Fe or Mn (μmole cm^{-3})

ΣR = general reaction term for Fe or Mn reduction (μmole cm^{-3} yr^{-1})

D_b = particle mixing rate (cm^2 yr^{-1})

If it is assumed that Fe or Mn reduction is the only reaction occurring, then the reduction rate can be defined as the depth-integrated sum of reactions, expressed as:

$$\int_{z_1}^{z_2} \Sigma R_{(z)} dz = D_b \int_{z1}^{z2} \frac{d^2 C}{dz^2} dz \quad (6)$$

The second derivative of the fitted profiles was integrated over the zone of metal reduction. For Fe, this was from the bottom of the pore-water nitrate penetration depth (z_1) to the depth where excess concentrations reached zero (z_2); and for Mn, from the bottom of the pore-water oxygen penetration depth (z_1) to the depth where excess Mn concentrations reached zero (z_2). This quantity was multiplied by the bioturbation rate determined from the ^{234}Th profile from the same station to calculate the Fe and Mn reduction rate. For Fe calculations, three stations (Table 4) had no usable pore-water nitrate profile, in which case the bottom of the Mn reduction zone was used for z_1.

The relative contribution of Fe or Mn oxide reduction to OM remineralization was estimated using the calculated Fe or Mn reduction rates and the measured oxygen flux

rates from incubation cores. Total carbon oxidation rates were estimated from sediment oxygen consumption rates, based on Redfield ratio $C_{org}:O_2 = 106:138$. The fraction of OM remineralized by Fe or Mn oxide reduction was then determined by assuming the stoichiometric ratios of 4Fe: $1C_{org}$ and 2Mn:$1C_{org}$ (Table 1, Froelich et al. 1979).

c. Soluble Iron and Manganese in the Pore-water

Pore-water samples that were frozen for Fe and Mn analysis were allowed to slowly thaw under refrigeration at approximately 4°C and then diluted with nitric acid to achieve a 1.5% or 2% solution, depending on sample volume. Acidified samples were analyzed using flame atomic absorption spectrophotometry, as previously described.

2.3. Statistical Analyses

To determine the extent to which rates of both Fe and Mn oxide reduction positively covaried with sediment oxygen consumption rates, linear regressions were performed on full datasets, using the statistical program R (Free Software Foundation, Inc.). In order to satisfy the normality assumption for linear regression, Fe and Mn oxide reduction rates were log transformed prior to statistical analysis. The linear regressions shown are significant at the $\alpha = 0.05$ level.

Additionally, Jonckheere's test for ordered alternatives was used to test the hypothesis of no difference among shelf regions against the ordered alternative, $\tau_1 > \tau_2 > \tau_3 > \tau_4$ (Hollander and Wolfe 1973). That is, regions will follow the predicted order: northern shelf > middle shelf > outer shelf > off shelf, with the highest rates in the northern region, where the tightest benthic-pelagic coupling is expected.

Table 2. Sampling locations in the Bering Sea for both HLY0902 and KN195-10.

Date	Station	Depth (m)	Location
	Northern-Shelf Region		
4/16/2009	HLY 32	80	62° 11.924'N 175° 8.463'W
4/16/2009	HLY 35	62	61° 57.693'N 173° 14.382'W
4/17/2009	HLY 39	51	61° 56.049'N 171° 12.878'W
5/1/2009	HLY 92	72	61° 34.3'N 173° 42.75'W
5/2/2009	HLY 93	57	62° 15.98'N 172° 31.04'W
5/4/2009	HLY 98	81	62° 10.94'N 175° 8.69'W
7/6/2009	KNR 130	65	61° 0.003'N 171° 45.324'W
7/7/2009	KNR 137	51	62° 12.063'N 171° 53.391'W
7/7/2009	KNR 140	62	62° 12.076'N 173° 6.379'W
7/8/2009	KNR 147	95	62° 11.983'N 175° 58.513'W
	Middle-Shelf Region		
4/7/2009	HLY 9	55	59° 58.193'N 169° 51.856'W
4/21/2009	HLY 54	68	58° 22.093'N 168° 43.91'W
4/22/2009	HLY 58	67	57° 27.08'N 169° 45.194'W
4/28/2009	HLY 83	91	60° 48.78'N 174° 23.38'W
6/22/2009	KNR 45	70	57° 53.93'N 169° 14.49'W
6/30/2009	KNR 89	66	59° 42.86'N 170° 19.27'W
	Outer-Shelf Region		
4/9/2009	HLY 17	104	59° 54.23'N 173° 59.23'W
4/10/2009	HLY 19	120	59° 51.305'N 175° 13.41'W
4/23/2009	HLY 65	109	56° 43.41'N 170° 31.86'W
4/26/2009	HLY 69	133	59° 33.79'N 175° 12.05'W
4/27/2009	HLY 73	129	59° 35.428'N 175° 4.62'W
4/30/2009	HLY 90	132	59° 32.75'N 175° 8.95'W
5/16/2009	HLY 116	130	59° 33.709'N 175° 9.17'W
6/18/2009	KNR 22	113	56° 7.694'N 166° 7.836'W
6/20/2009	KNR 32	104	56° 48.154'N 167° 52.25'W
6/25/2009	KNR 60	196	57° 16.747'N 173° 50.522'W
6/29/2009	KNR 79	121	57° 9.839'N 172° 56.764'W
7/2/2009	KNR 106	105	59° 54.00'N 173° 59.981'W
7/3/2009	KNR 113	152	59° 53.683'N 178° 44.589'W
7/5/2009	KNR 122	136	59° 33.803'N 175° 11.998'W
	Off-Shelf Region		
4/12/2009	HLY 25	705	59° 53.55'N 178° 54.198'W
4/12/2009	HLY 26	2714	59° 55.059'N 179° 27.253'W
6/14/2009	KNR 1	1246	54° 14.744'N 166° 33.838'W
6/19/2009	KNR 27	2343	55° 1.394'N 169° 13.02'W
6/23/2009	KNR 53	2800	56° 3.817'N 171° 20.268'W
6/26/2009	KNR 67	3492	57° 29.751'N 175° 14.567'W

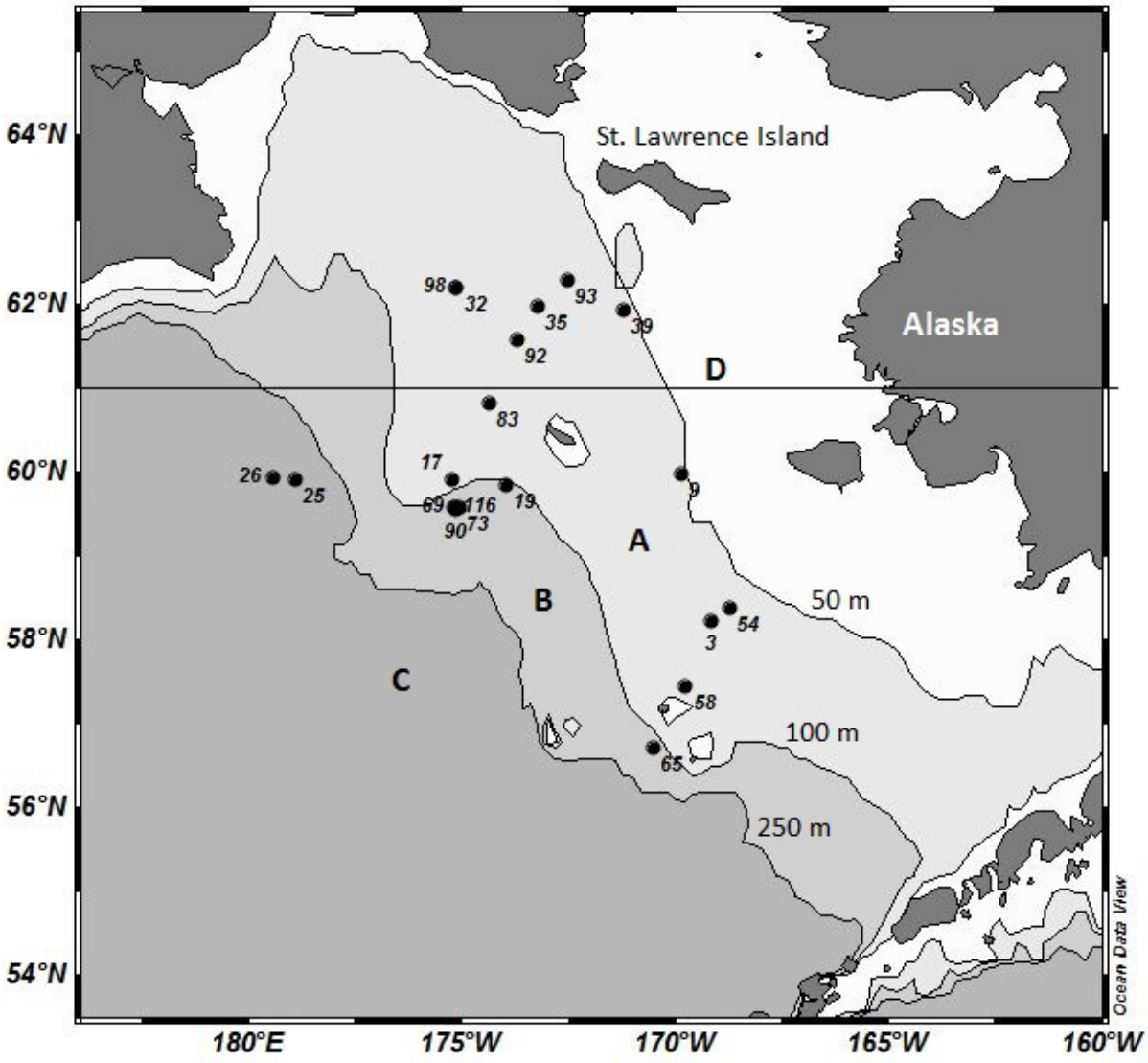

Fig. 2. Spring sampling locations in the Bering Sea (HLY0902). Bathymetry lines indicate the locations of oceanographic fronts that separate the shelf into the middle (A) and outer (B) regions. Past the shelf break is the off-shelf region (C) and the northern region (D) is located above 61° latitude.

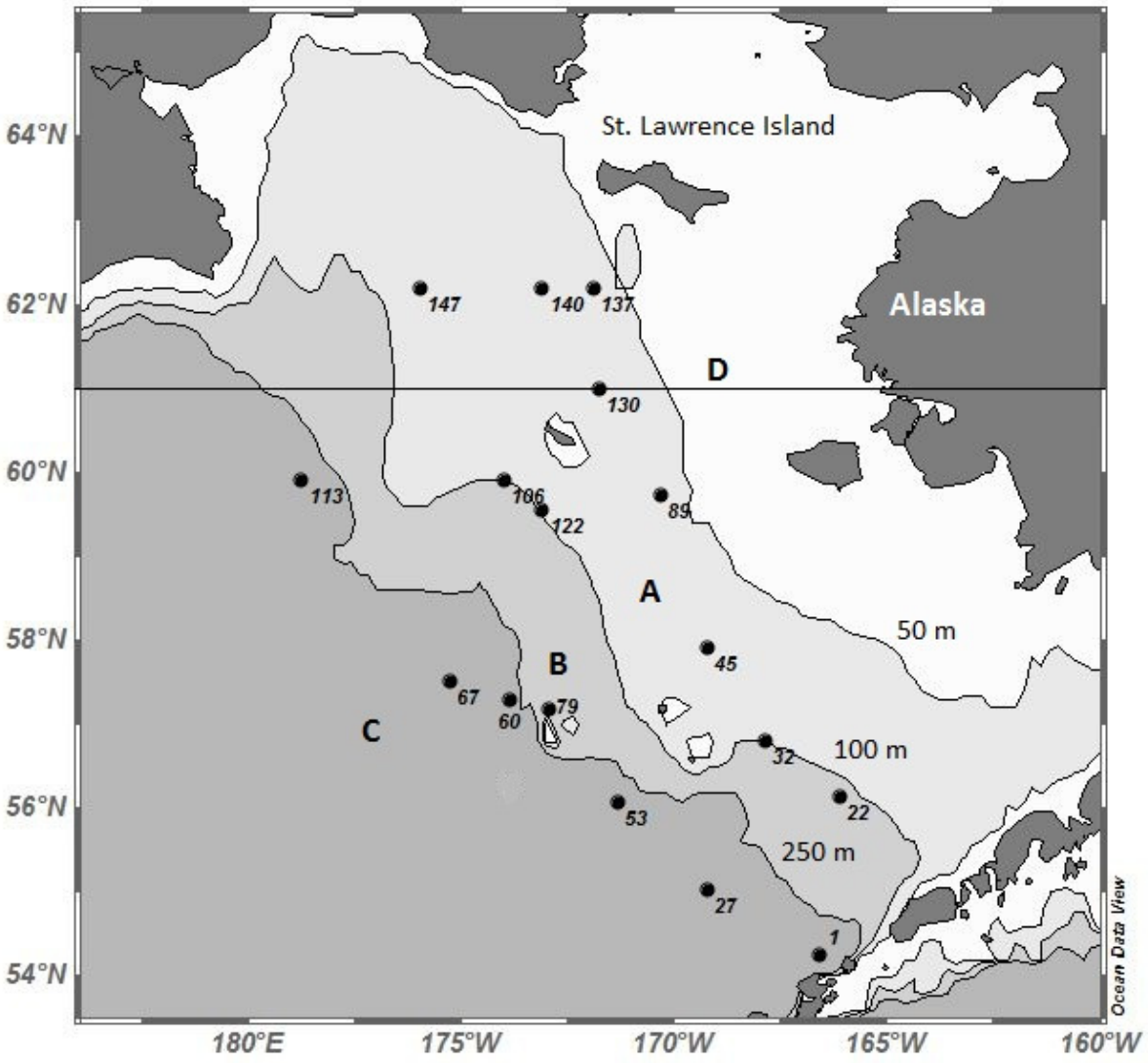

Fig. 3. Summer sampling locations in the Bering Sea (KN195-10). Bathymetry lines indicate the locations of oceanographic fronts that separate the shelf into the middle (A) and outer (B) regions. Past the shelf break is the off-shelf region (C) and the northern region (D) is located above 61° latitude.

3.0 Results

3.1 Bioturbation

Bioturbation rates, determined from excess ^{234}Th profiles (Fig. 4, Appendix A) varied across the shelf (Table 3). The highest rates, on average, were in the northern region (mean: 6.29 cm^2 yr^{-1}), while the off-shelf region was characterized by very low rates of bioturbation (mean: 1.37 cm^2 yr^{-1}), with the exception of station KNR 53, which had a rate of 4.79 cm^2 yr^{-1} (Fig. 5). Average bioturbation rates for the middle and outer-shelf regions fell in between the northern and off-shelf regions (3.43 and 2.42 cm^2 yr^{-1}, respectively).

The range of bioturbation rates calculated for the northern and middle-shelf regions were fairly wide and overlapped to some degree. The outer and off-shelf regions had more narrow ranges, comparatively, although they both had outliers on the high end of their range. These outliers may be a result of 'hotspots' of high benthic faunal activity (Fig. 5).

Table 3. Bioturbation rates for each sampling location in the Bering Sea.

Date	Station	Depth (m)	Db ($cm^2\ yr^{-1}$)	Fauna (ind. m^{-2})
		Northern Shelf Region		
4/16/2009	HLY 32	80	4.36	161
4/16/2009	HLY 35	62	11.09	265
4/17/2009	HLY 39	51	6.30	126
5/1/2009	HLY 92	72	5.69	226
5/2/2009	HLY 93	57	5.27	67
5/4/2009	HLY 98	81	1.59	216
7/6/2009	KNR 130	65	5.55	1027
7/7/2009	KNR 137	51	11.83	565
7/7/2009	KNR 140	62	9.22	429
7/8/2009	KNR 147	95	2.02	139
		Middle Shelf Region		
4/7/2009	HLY 9	55	7.75	127
4/21/2009	HLY 54	68	1.14	368
4/22/2009	HLY 58	67	5.41	96
4/28/2009	HLY 83	91	2.04	452
6/22/2009	KNR 45	70	2.04	415
6/30/2009	KNR 89	66	2.16	1365
		Outer Shelf Region		
4/9/2009	HLY 17	104	1.17	67
4/10/2009	HLY 19	120	7.30	106
4/23/2009	HLY 65	109	2.17	99
4/26/2009	HLY 69	133	3.04	80
4/27/2009	HLY 73	129	1.37	122
4/30/2009	HLY 90	132	0.63	65
5/16/2009	HLY 116	130	2.83	121
6/18/2009	KNR 22	113	3.04	241
6/20/2009	KNR 32	104	3.75	325
6/25/2009	KNR 60	196	0.15	136
6/29/2009	KNR 79	121	1.27	120
7/2/2009	KNR 106	105	2.02	132
7/3/2009	KNR 113	152	1.62	124
7/5/2009	KNR 122	136	3.55	57
		Off Shelf Region		
4/12/2009	HLY 25	705	0.647	32
4/12/2009	HLY 26	2714	0.899	20
6/14/2009	KNR 1	1246	1.23	56
6/19/2009	KNR 27	2343	0.354	30
6/23/2009	KNR 53	2800	4.786	44
6/26/2009	KNR 67	3492	0.314	21

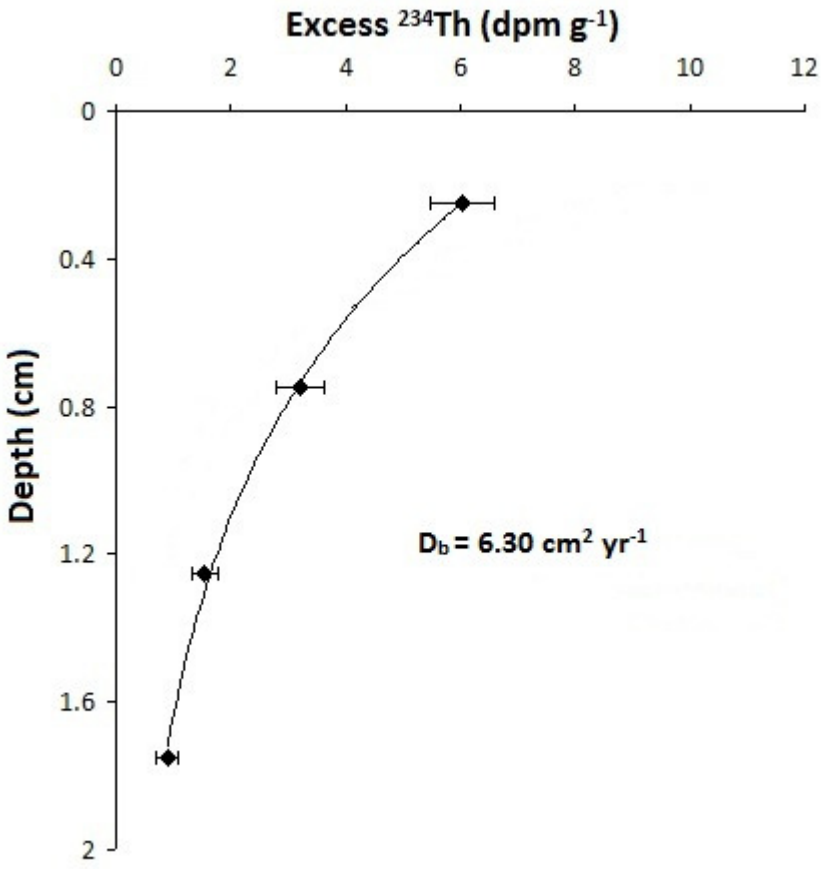

Figure 4. Example of an excess ^{234}Th profile used to determine rates of bioturbation (D_b). Station profile shown is HLY 39.

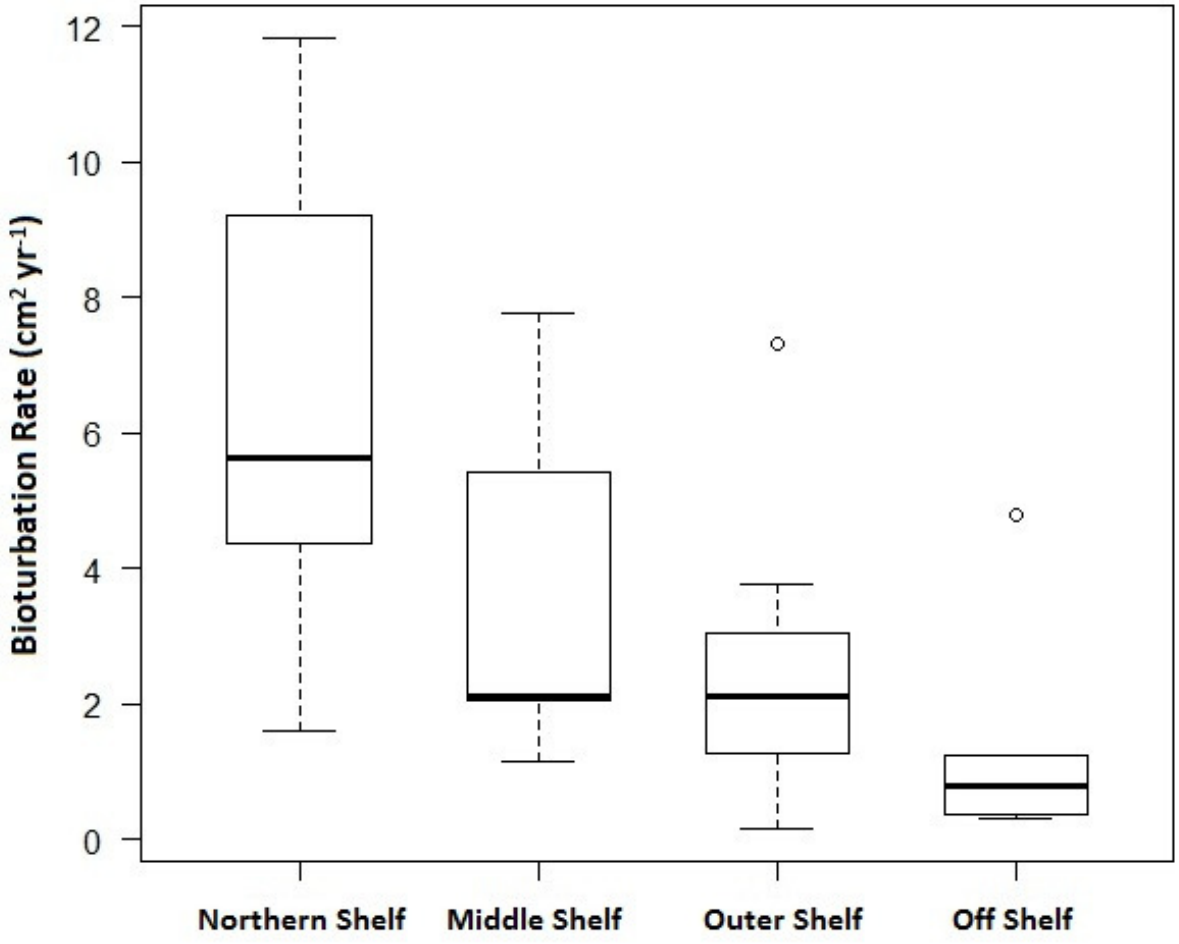

Figure 5. Box and whisker plot showing bioturbation rates separated by shelf region.

3.2 Solid-phase Iron and Manganese

There were no defining characteristics of the AAO-extracted solid-phase Fe profiles specific to shelf region. In general, the profiles showed a subsurface peak within approximately the first centimeter, an immediate decrease in Fe oxide concentrations right below the sediment-water interface, or no gradient at all (Fig. 6, Appendix A). Solid-phase Mn profiles, on the other hand, either had a very steep, shallow gradient just below the sediment surface, generally associated with higher surface concentrations of Mn oxides, or a more gradual decrease in Mn oxide concentration (Fig. 7, Appendix A).

The oxidation of organic carbon by Fe and Mn oxides results in the reduction of these metals to their soluble phase, such that the increase of Fe^{2+} and Mn^{2+} in pore-water provides another indication of Fe and Mn oxide reduction. At stations where both solid-phase and pore-water Fe and Mn profiles were available, comparisons showed that the depth range over which oxide concentrations decreased was consistent with the depth range over which Fe and Mn pore-water concentrations increased, thereby confirming the relative depth distributions of Fe or Mn reduction.

Pore-water nitrate profiles were also compared to profiles of pore-water Fe and Mn (Fig. 8, Table 4). Side-by-side analyses showed that Mn oxide reduction, if significant, was occurring very close to the sediment-water interface, usually overlapping with the zone of denitrification, as can often occur (Froelich et al. 1979, Burdige 1993, Emerson and Hedges 2003). Additionally, Fe oxide reduction typically began at the depth where pore-water nitrate concentrations were at, or near zero. These comparisons indicate that the integration limits I chose (representing the depth range of Fe or Mn reduction) to calculate rates of Fe and Mn oxide reduction were reasonable.

The rates of Fe and Mn oxide reduction were also analyzed separately by region, but in general, rates of Fe oxide reduction across the southeastern Bering Sea were much higher than those calculated for Mn oxide reduction. Rates of sedimentary Fe reduction showed a regional trend similar to that of the bioturbation rates (Fig. 9), with the highest rates in the northern and middle-shelf regions (mean rates: 4.14, 1.76 mmole m^{-2} d^{-1}, respectively), and the lowest in the outer and off-shelf regions (mean rates: 0.90, 0.36 mmole m^{-2} d^{-1}, respectively). Although the mean rate of Fe reduction across all regions of the shelf was approximately 1.74 mmole m^{-2} d^{-1}, the highest rate of Fe reduction was greater than 9 mmole m^{-2} d^{-1}.

In contrast to Fe, rates of Mn oxide reduction were consistently low across the shelf (Table 4, Fig. 10). The highest average rates of Mn reduction were, again, in the northern and middle-shelf regions (means: 0.21 mmole m^{-2} d^{-1}, 0.11 mmole m^{-2} d^{-1}, respectively), but unlike Fe reduction rates, the off-shelf region had slightly higher Mn reduction rates than the outer shelf (means: 0.08 mmole m^{-2} d^{-1}, 0.02 mmole m^{-2} d^{-1}, respectively).

The percentage of OM remineralized by Fe oxide reduction followed the same trend as Fe reduction (Fig. 9), and on average accounted for about 7% of carbon oxidation across all regions. Percentages of carbon oxidized by Fe reduction in the northern-shelf region encompassed the widest range, from approximately 3% to slightly over 36%. The percentages calculated in the middle-shelf region were comparable to the low-end of the northern region's range. The ranges of percentages for the outer and off-shelf regions were similar and contained some of the lowest calculated values.

The fraction of OM remineralization attributed to Mn oxide reduction was extremely low across the shelf. Average percentages of carbon remineralized by Mn oxide reduction were not above 5% in any region (Fig. 10). The highest calculated percentages were spread across the northern, middle and off-shelf regions. These stations also had relatively high surface concentrations of Mn oxides, possibly pointing to low reduction rates of Mn oxides in this region (Table 4).

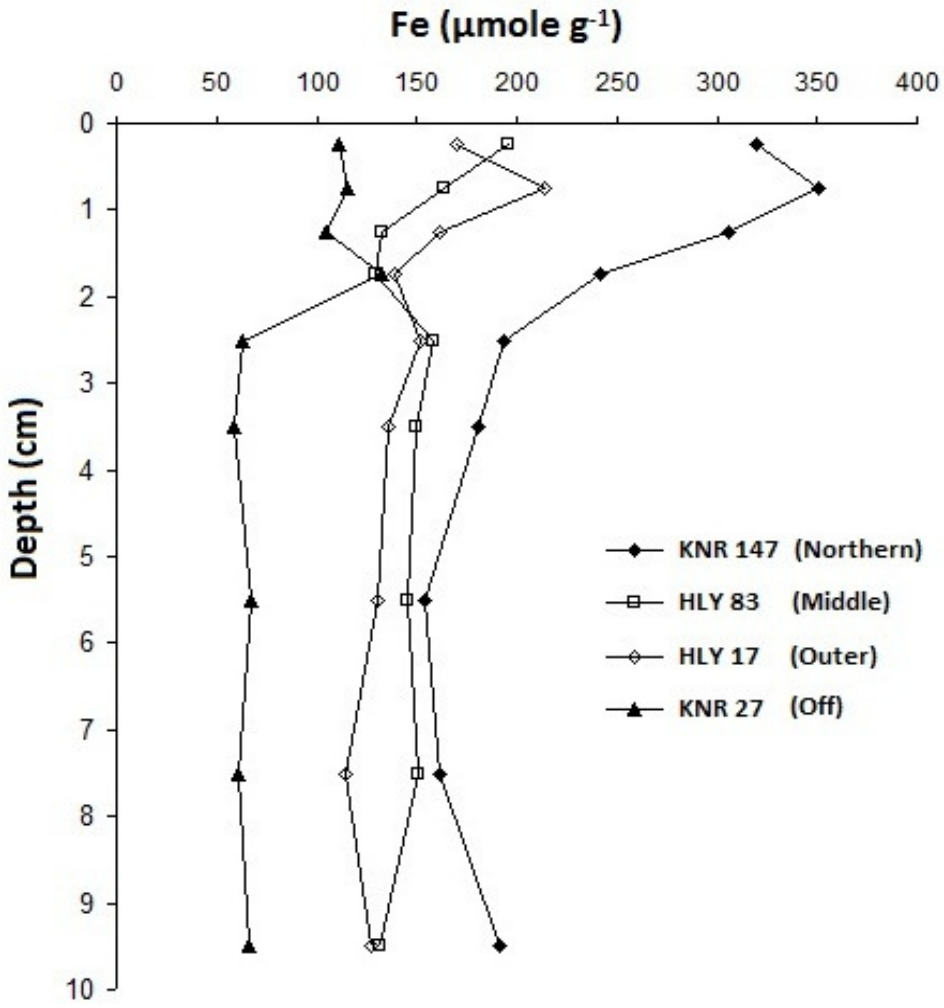

Figure 6. Examples of AAO-extracted Fe oxide concentration profiles. One station from each region of the southeastern Bering Sea is shown.

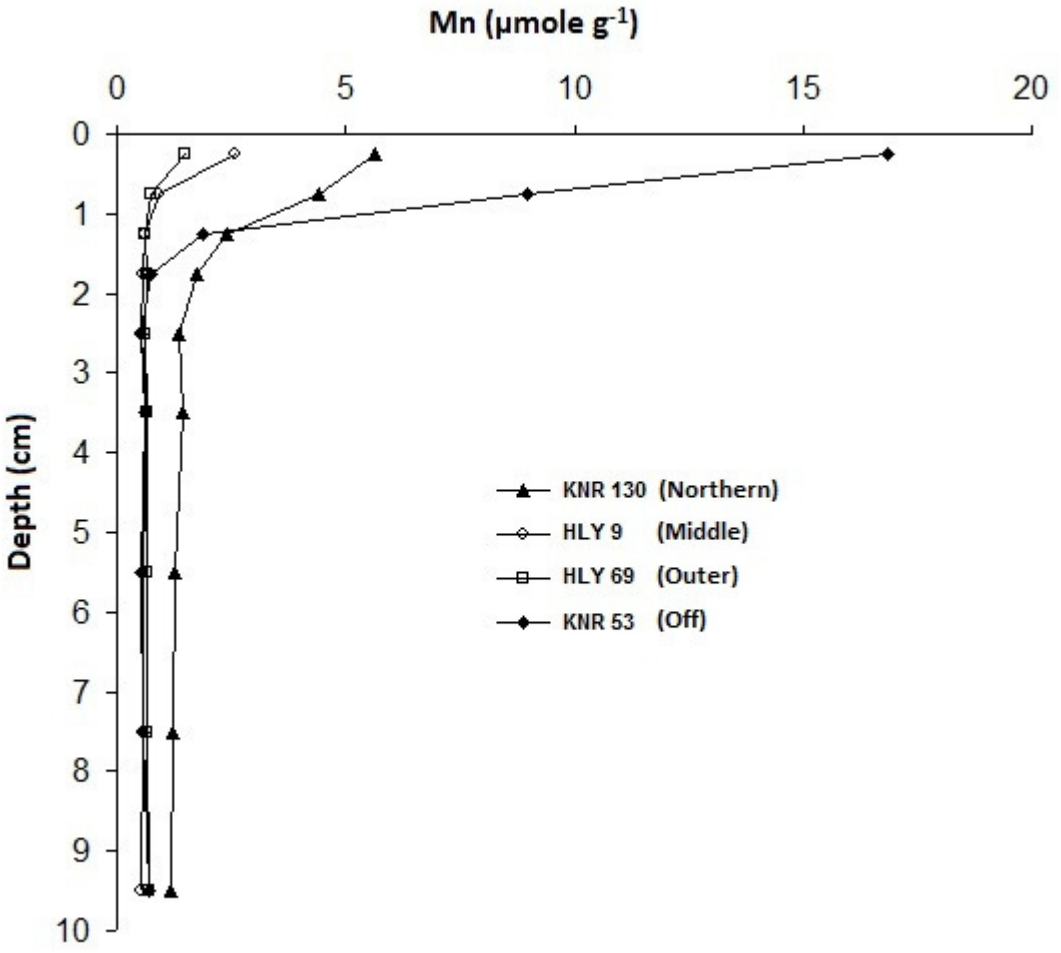

Figure 7. Examples of AAO-extracted Mn oxide concentration profiles. One station from each region of the southeastern Bering Sea is shown.

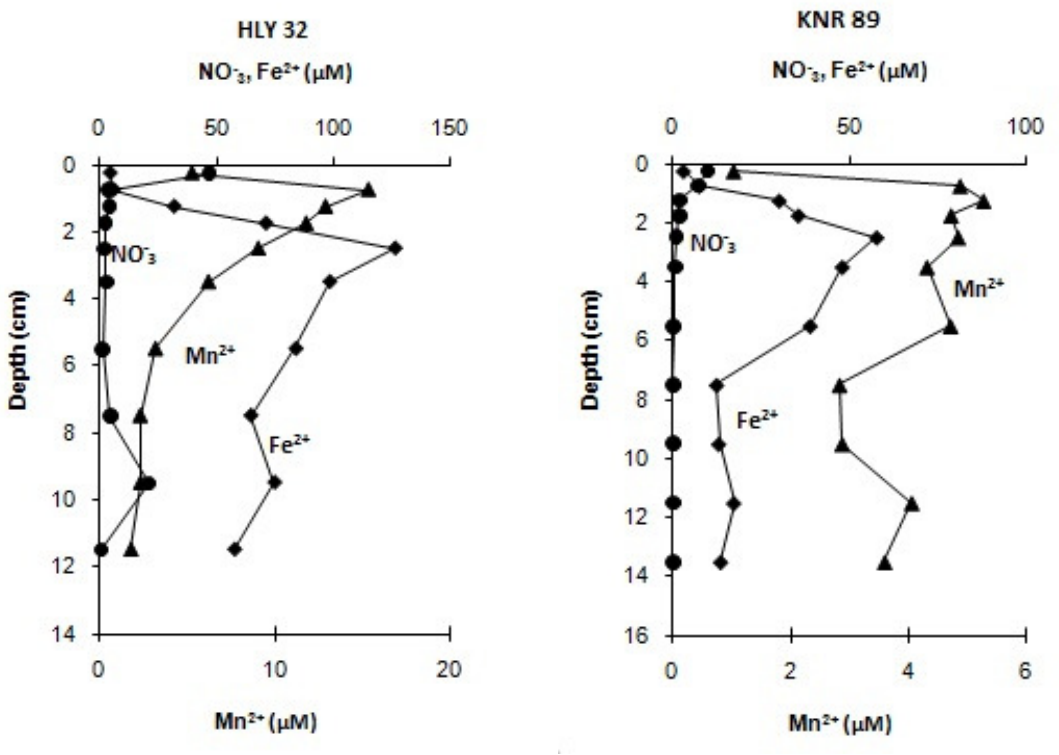

Figure 8. Examples of pore-water profiles of Fe^{2+}, Mn^{2+} and NO^{-}_{3} used to show the overlap of Mn reduction with denitrification as well as the initiation of Fe reduction once pore water nitrate concentrations are at or near zero. The profiles depicted are from stations HLY 32 and KNR 89.

Table 4. A summary of measured sediment properties as well as calculated metal reduction rates. Percent of total organic carbon oxidation in parentheses. "No fit" indicates Fe/Mn profiles for which an appropriate model fit could not be found.

Station	O_2 flux (mmole m^{-2} d^{-1})	O_2 P.D. (cm)	NO^- P.D. (cm)	*Total C_{oxid} (mmole m^{-2} d^{-1})	Fe Red. Rate (mmole m^{-2} d^{-1})	Mn Red. Rate (mmole m^{-2} d^{-1})	Surface Fe (umoles g^{-1})	Surface Mn (umoles g^{-1})
Northern Shelf Region								
HLY 32	5.96	0.75	2.50	4.58	0.89 (4.84)	0.34 (3.76)	166.8	1.97
HLY 35	8.41	1.15	5.50	6.46	9.46 (36.59)	0.57 (4.41)	102.75	1.97
HLY 39	6.22	0.65	1.75	4.78	5.08 (26.59)	0.08 (0.86)	92.56	2.69
HLY 92	7.61	1.05	1.25	5.84	4.30 (18.41)	0.22 (1.84)	193.02	3.64
HLY 93	8.20	0.50	2.50	6.30	No fit	0.03 (0.21)	104.74	1.64
HLY 98	10.03	0.95	1.25	7.71	1.00 (3.25)	0.01 (0.04)	159.21	1.89
KNR 130	16.57	0.45	0.75	12.73	6.31 (12.40)	0.09 (0.37)	218.77	5.66
KNR 140	9.75	0.55	1.75	7.49	No fit	No fit	102.57	1.71
KNR 147	10.38	0.50	1.25	7.97	1.97 (6.18)	0.02 (0.11)	319.72	2.17
Middle Shelf Region								
HLY 9	7.61	1.35	2.5	5.85	3.46 (14.80)	0.39 (3.31)	143.08	2.59
HLY 54	10.19	1.25	--	7.83	1.75 (5.58)	0.01 (0.06)	120.22	1.86
HLY 58	7.83	0.60	--	6.01	No fit	0.04 (0.34)	73.52	0.89
HLY 83	8.73	0.75	1.25	6.71	1.59 (5.91)	0.07 (0.49)	195.54	3.04
KNR 45	11.46	0.50	--	8.80	1.07 (6.56)	0.02 (0.13)	89.65	1.19
KNR 89	7.90	0.80	1.75	6.07	0.96 (3.95)	0.12 (1.01)	163.02	2.97
Outer Shelf Region								
HLY 17	5.41	1.25	1.25	4.15	0.93 (5.62)	0.00 (0.05)	170.04	2.37
HLY 19	6.99	1.05	1.75	5.37	0.90 (4.21)	No fit	111.29	1.07
HLY 65	4.50	1.25	1.75	3.45	0.31 (2.25)	0.02 (0.34)	81.78	0.89
HLY 69	4.76	0.85	5.50	3.65	No fit	0.04 (0.60)	139.52	1.49
HLY 73	5.98	1.10	1.25	4.60	0.87 (4.76)	0.00 (0.01)	83.84	1.75
HLY 90	5.78	1.55	1.75	4.44	0.11 (0.62)	0.00 (0.01)	103.27	1.17
HLY 116	6.68	0.95	5.50	5.13	1.46 (7.10)	0.04 (0.41)	105.74	1.06
KNR 22	9.38	0.70	3.50	4.94	0.31 (1.07)	No fit	119.64	0.86
KNR 32	7.88	0.65	1.75	6.06	3.65 (15.07)	0.10 (0.82)	111.02	1.06
KNR 60	5.83	0.30	--	4.47	0.04 (0.24)	0.00 (0.02)	29.38	0.17
KNR 79	10.54	1.15	1.75	8.10	0.48 (1.48)	0.02 (0.10)	62.85	1.18
KNR 106	11.89	0.60	3.50	9.13	No fit	0.01 (0.04)	143.32	1.53
KNR 113	6.10	1.15	1.75	4.69	0.53 (2.84)	0.01 (0.11)	56.1	0.67
KNR 122	8.62	0.85	2.50	6.62	1.14 (4.30)	0.02 (0.18)	105.18	0.98
Off Shelf								
HLY 25	3.70	0.50	0.75	2.84	0.45 (3.98)	No fit	76.01	0.75
HLY 26	3.25	0.50	7.50	2.49	No fit	0.03 (0.58)	81.74	5.35
KNR 1	1.24	0.55	2.50	0.96	0.08 (2.22)	0.01 (0.34)	126.49	1.69
KNR 27	6.44	0.80	2.50	4.94	0.22 (1.10)	No fit	111.31	17.53
KNR 53	5.33	0.85	2.50	4.09	0.95 (5.82)	0.26 (3.22)	156.3	16.83
KNR 67	4.38	0.90	2.00	3.37	0.11 (0.83)	0.01 (0.21)	106.61	28.57

*Total carbon oxidation rates based on oxygen flux rates.

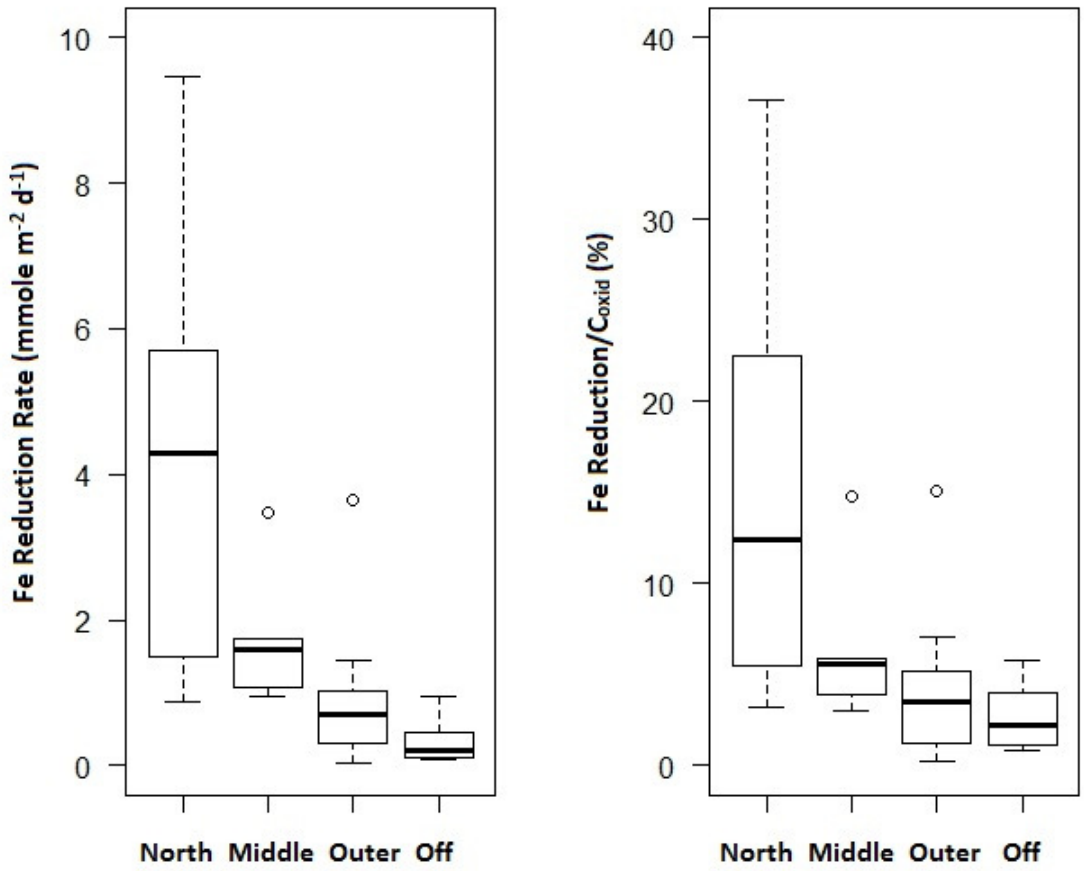

Figure 9. Box and whisker plots of iron reduction rates by region and as a percentage of total carbon oxidation rates based oxygen consumption rates.

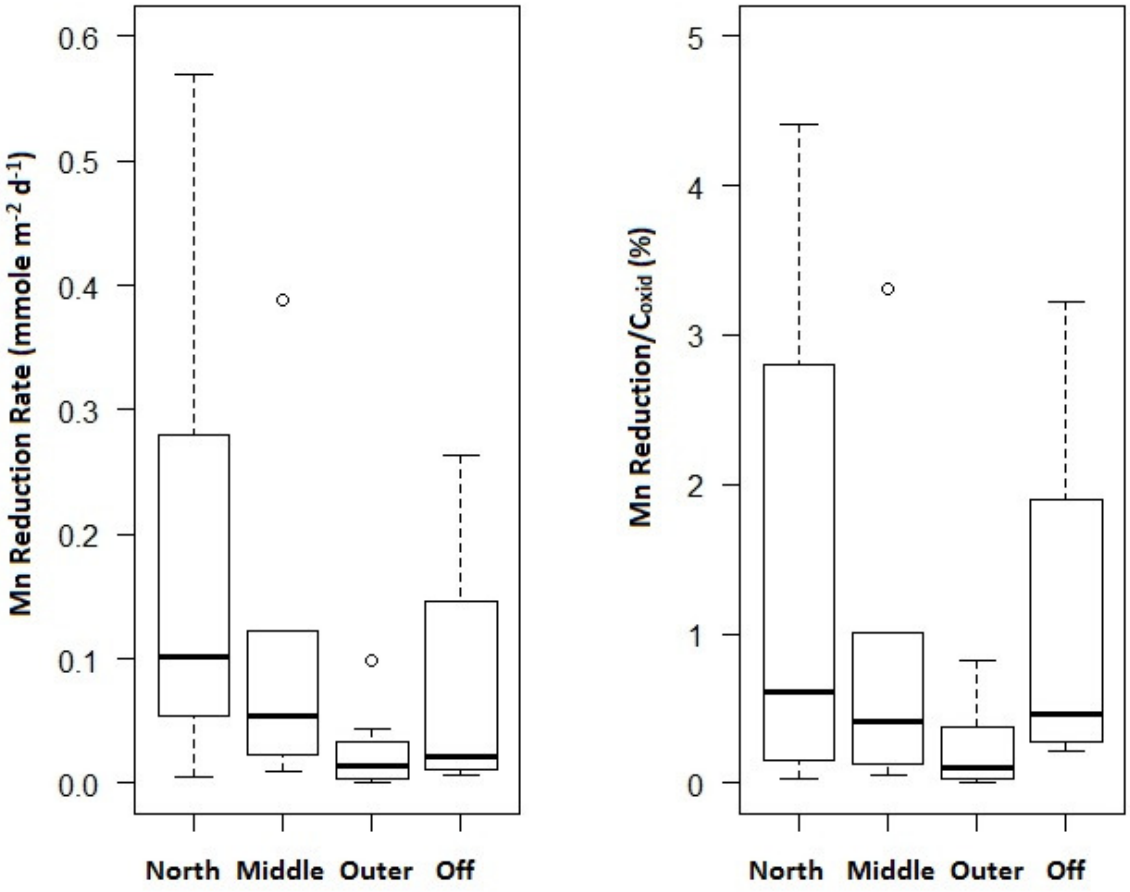

Figure 10. Box and whisker plots showing Mn reduction rates by region and as a percentage of total carbon oxidation rates, based oxygen consumption rates.

3.3 Statistical Analyses

A significant linear relationship was found between rates of Fe oxide reduction and sediment oxygen consumption rates ($p = 0.003$; Fig. 11). However, there is a reasonably large amount of variation in Fe reduction rates within the median range of oxygen flux rates. Furthermore, based on the regression analysis, oxygen flux can account for only approximately 26% of the variation in Fe reduction ($R^2 = 0.26$). Regarding Mn reduction, there was no discernable relationship between Mn reduction rates and sediment oxygen consumption rates, and linear regression analysis found no significant correlation between these variables (Fig. 12).

Jonckheere's test for ordered alternatives resulted in the rejection of the null hypothesis of no difference among shelf regions for both Fe reduction ($J^* = -4.06$, $p < 0.0001$), and the percentage of OM remineralized by the reduction of Fe oxides ($J^* = -3.07$, $p = 0.0011$). The alternative was that reduction rates would decrease from the northern to the off-shelf region such that the regions would be ordered as: northern shelf > middle shelf > outer shelf > off shelf. Manganese reduction rates were also found to follow the predicted order ($J^* = -2.11$, $p = 0.0174$). However, the percentages of OM remineralized by Mn reduction was not found to significantly differ from region to region ($J^* = -1.02$, $p = 0.1539$).

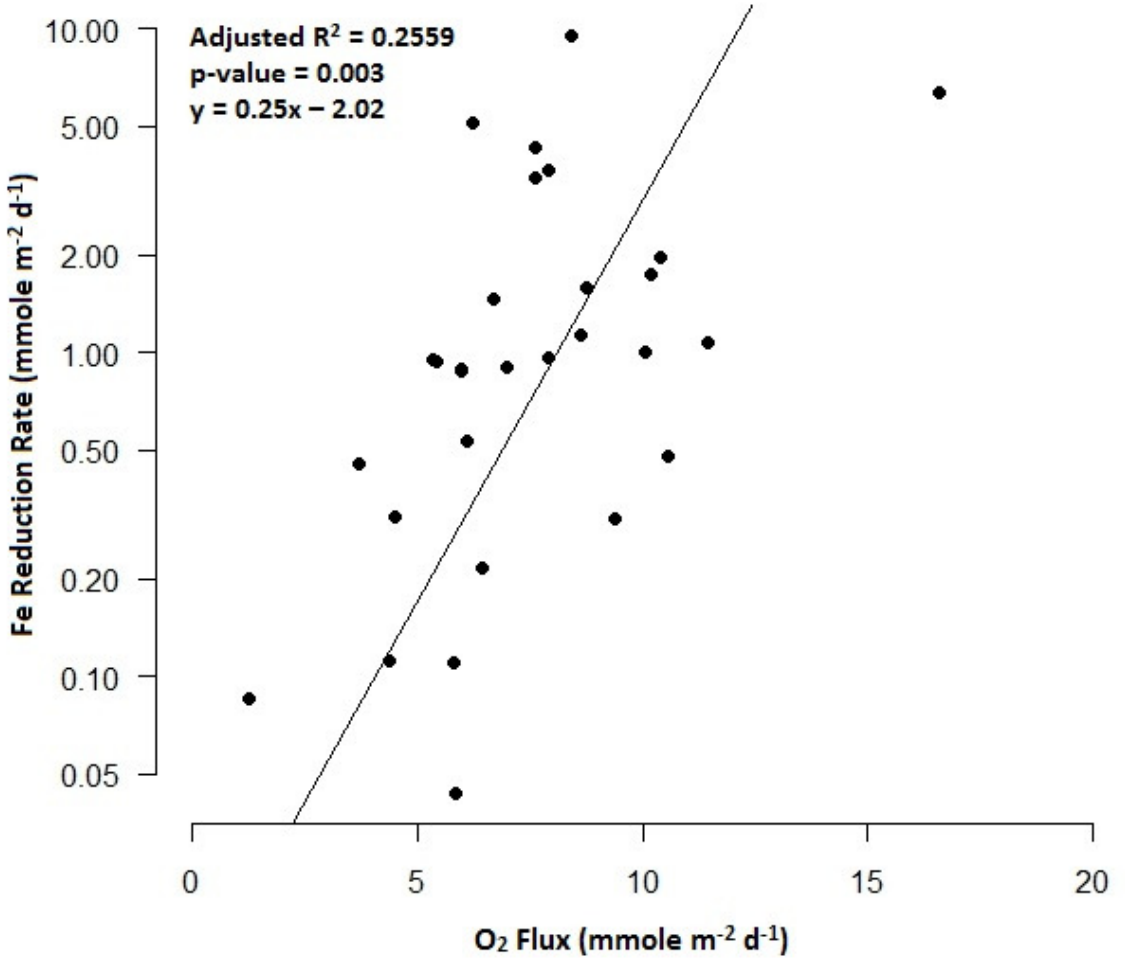

Figure 11. Rates of iron oxide reduction plotted as a function of total oxygen consumption rates across the southeastern Bering Sea shelf. Iron oxide reduction rates are plotted on a log scale.

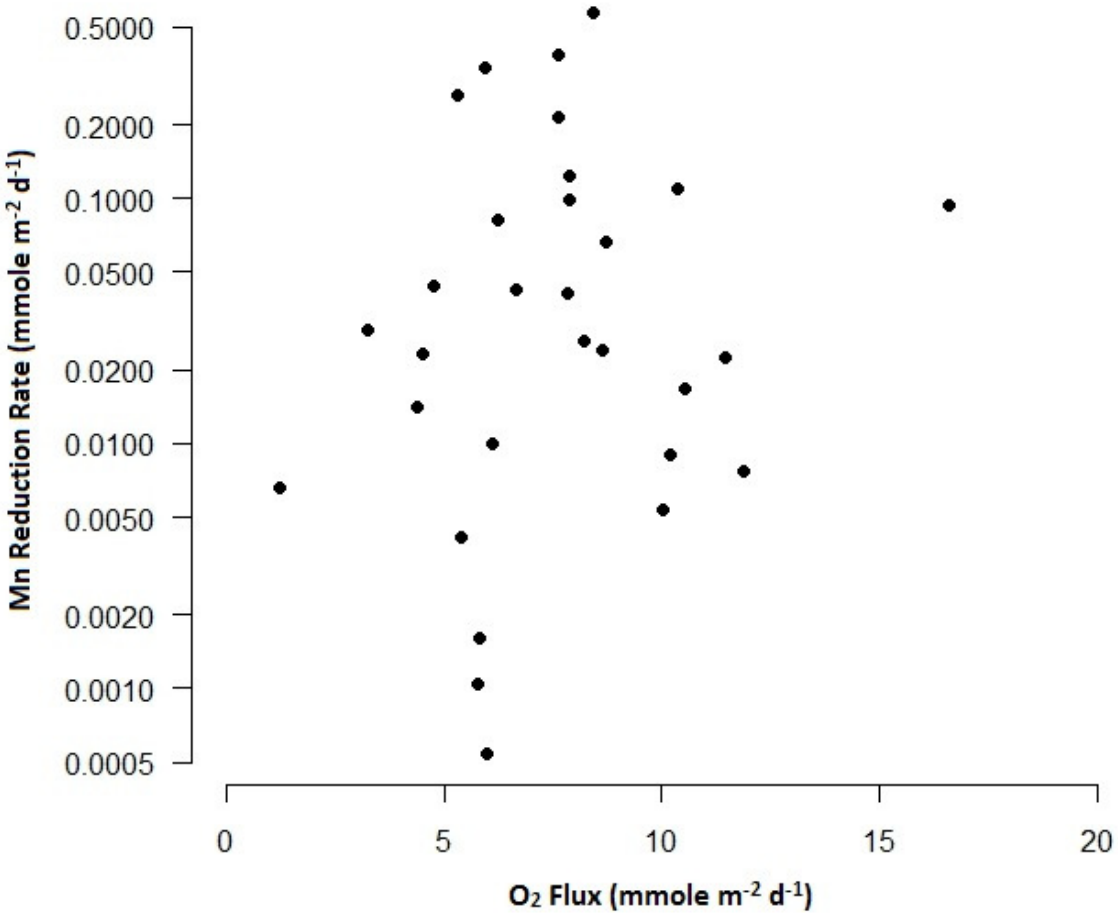

Figure 12. Rates of manganese oxide reduction plotted as a function of total oxygen consumption rates across the southeastern Bering Sea shelf. Manganese oxide reduction rates are plotted on a log scale.

4.0 Discussion

I expected rates of Fe and Mn reduction to vary regionally across the shelf, following the pattern: northern shelf > middle shelf > outer shelf > off shelf. Consistent with this hypothesis, rates of both Fe reduction and bioturbation varied as expected. In contrast, the cross-shelf variation in Mn reduction rates did not show as strong a pattern, likely due to very low calculated rates of Mn reduction in all regions. However, to determine both Fe and Mn reduction rates an estimated rate of bioturbation, or D_b was required.

4.1 Bioturbation

The method of quantifying bioturbation rates by fitting a diffusive model to the profile of particle-reactive radionuclide tracer requires several assumptions (Meysman et al. 2003, Burdige 2006). First, the calculation of a biodiffusion coefficient (D_b) requires that particle mixing be spatially random and occur over a small scale, analogous to diffusive transport. That is, the distance over which particle movement occurs is shorter than the tracer's mixing length. Second, the frequency of mixing events must be more frequent than the decay rate of the tracer. Short-lived radioisotopes, such as ^{234}Th, may violate these assumptions. Smith et al. (1993) found a strong negative correlation between tracer half-life and bioturbation rate, a relationship which can be referred to as tracer dependence. More recently, tracer dependence has been shown to be of greater significance in sediments with low mixing rates. Lecroart et al. (2010) argued that in environments with bioturbation rates greater than 2 $cm^2\ yr^{-1}$, tracer dependence is absent and ^{234}Th is suitable to quantify values of D_b. Bioturbation rates calculated in this study meet that condition in all the regions of the Bering Sea, except for the off-shelf region,

which had an average bioturbation rate of 1.37 cm^2 yr^{-1}, the lowest of all the regions. Without the somewhat anomalous station, KNR 53, the off-shelf region's average bioturbation rate drops even lower, to approximately 0.7 cm^2 yr^{-1}. Thus, it is likely that the very low values of D_b calculated for the off-shelf region are overestimates of bioturbation. Since D_b was used in the calculation of Fe and Mn reduction rates, many of the calculated rates in the off-shelf region are likely overestimated as well. Regardless, D_b is still a good indicator of variation in bioturbation, even in the off-shelf region. This region also had low organism counts from benthic fauna samples (Table 3), and the lowest mean rate of sediment oxygen consumption (Table 4), all likely explained by a low flux of OM to the sediment surface associated with greater water depths found in this region.

On the other hand, the highest rates calculated were found in the northern-shelf region, as expected. It has been noted that this region has tight benthic-pelagic coupling, with high quality OM deposited to the sediment surface, supporting high benthic biomass and therefore high rates of particle-mixing (Grebmeier et al. 1988, 2006). The range of bioturbation rates in the middle-shelf region included rates similar to those found in the northern-shelf region (Fig. 5), pointing to comparable environmental conditions. In fact, Grebmeier et al. (1988) described the middle-shelf region as similar to the northern region, with tight benthic-pelagic coupling and relatively high rates of OM deposition. However, this is in contrast to the outer-shelf region where pelagic grazing dominates and less OM is delivered to the sediment surface (Grebmeier et al. 1988). It is therefore not surprising that this region had the second lowest average calculated D_b.

The trend, northern shelf > middle shelf > outer shelf > off shelf, observed in bioturbation rates across the shelf follows the expected variation in benthic-pelagic coupling. However, the stations with the highest rates of bioturbation did not necessarily have the highest faunal abundances (Table 3), suggesting that factors other than just organism abundance influence bioturbation rates, such as benthic community composition. More specifically, the relative trophic structure of the benthic community, and specific feeding strategies of the organisms present, may more directly affect rates of bioturbation (Dauwe et al. 1998).

4.2 Iron and Manganese Reduction

Iron and Mn oxide reduction have historically been thought of as minor contributors to OM remineralization; however, more recent studies have shown that Fe and Mn oxide reduction can be important components of sediment carbon respiration in some marine sediment environments (Canfield et al. 1993b, Kostka et al. 1999, Nickel et al. 2008). Often, these environments are characterized by intermediate rates of OM deposition, high sediment concentrations of Fe and Mn oxides, and low sulfate reduction rates (Vandieken et al. 2006, Nickels et al. 2008).

a. Iron

High rates of Fe reduction corresponded to the regions of the Bering shelf where tight benthic-pelagic coupling is expected, in the northern and middle-shelf regions. Likewise, the lowest rates were in the off-shelf region where Fe oxide reduction accounted for less than 5% of total OM remineralization (Fig. 11, Table 4). Since this region includes the

deepest waters of the Bering Sea, with corresponding low OM fluxes to the sediments, it is not surprising that aerobic respiration is the dominant pathway for OM remineralization in the off-shelf region. Furthermore, bioturbation rates in this region are likely not high enough to support reduction of Fe and Mn oxides (Kostka et al. 1999, Table 3).

The average rate of Fe reduction in the outer shelf was only slightly higher than the off-shelf region, and mean percentages of Fe reduction for these regions were comparable (Fig. 11). It's possible that overestimated bioturbation rates in the off-shelf region lead to the overestimation of Fe reduction rates in this region. However, it may also suggest that, to an extent, areas of the outer-shelf region might be similar to the off-shelf region regarding factors regulating Fe reduction (i.e.: OM deposition, bioturbation rates, etc). Grebmeier et al. (1988) found low benthic biomass densities in the outer-shelf region and some of the rates of bioturbation calculated in the outer-shelf region were as low as rates seen in the off-shelf region (Table 3). Although there were some stations in the outer shelf where percentages of Fe reduction were comparably high, on average, the lower oxygen consumption rates (Table 4), and lower bioturbation rates in this region (Table 3) likely contribute to the decreased importance of Fe oxide reduction, compared to the middle and northern-shelf regions.

Overall, the pattern seen in both average Fe reduction rates and the percentage of carbon oxidation accounted for by Fe reduction across the shelf supports the hypothesis that rates should be higher in regions where greater OM export is expected, such as the northern and middle-shelf regions (Grebmeier et al. 2006). This is further supported by the results of Jonckheere's test for ordered alternatives. However, a number of the

stations in the northern and middle regions that had high rates of sediment oxygen consumption also had relatively low rates of Fe reduction. Under the assumption that a greater supply of OM to the benthos leads to enhanced rates of sediment oxygen uptake, I expected to see comparably high rates of metal oxide reduction at stations with high oxygen flux rates; yet, at those particular stations, rates of Fe reduction did not increase proportionally to oxygen consumption rates. Moreover, based on the results of the linear regression analysis between these variables, oxygen flux rates did not account for much of the variation in Fe reduction rates (Fig. 11). This suggests that other factors contribute to the variation in Fe reduction rates across the shelf. The similar trends seen in both bioturbation rates and rates of Fe reduction may be a result of the method used to calculate Fe reduction rates; still, bioturbation is likely a dominant factor influencing Fe reduction in Bering shelf sediments. Yet in order to more fully explain patterns of Fe reduction in the Bering Sea, further investigation into what is likely a complex interaction of environmental factors influencing rates of sedimentary Fe reduction is needed.

Nonetheless, based on the mean rate of Fe reduction I calculated (1.74 mmole m^{-2} d^{-1}), my findings suggest that sedimentary Fe reduction could supply a significant fraction of bioavailable iron to phytoplankton. Assuming an average rate of primary production of 250 g C yr^{-1} (Springer et al. 1996) and phytoplankton requirements of 0.01 moles Fe: 106 moles C (Brand 1991) if only 0.3% of reduced Fe were to leave the sediment by diffusion or bioirrigation, that would be sufficient to support phytoplankton growth. Thus it's possible that wintertime water-column mixing, frontal mixing processes or mixing along isopycnals at the shelf break could transport reduced Fe in

shelf bottom waters to surface waters, alleviating the Fe limitation on primary production across the shelf.

b. Manganese

The reduction of Mn oxides, on the other hand, tells a different story. A major reason for this may be the large difference in concentrations of Fe and Mn oxides, which may be one of the primary factors influencing their relative significance in carbon oxidation (Thamdrup 2000). Indeed, surface concentrations of Mn oxides were low across the shelf, except for a few stations in the off-shelf region (Table 4). Based on Jonckheere's test, Mn reduction rates by region were ordered as expected, but when compared to total carbon oxidation, no regional difference was found. Calculated rates of Mn reduction were very low in all regions and on average, accounted for less than 1% of total OM remineralization (Table 4, Fig. 10). In addition, excess Mn oxide concentrations, in general, were depleted within 2 cm of the surface. Thus, Mn oxide reduction is likely a minor pathway for OM remineralization in the southeastern Bering Sea (Thamdrup 2000, Vandieken et al. 2006).

The higher rate and percentage of Mn reduction seen at station KNR 53 in the off-shelf region may be due to the model overestimating the Mn oxide reduction rate based on the profile generated for this station. Half of the off-shelf stations had high surface concentrations of Mn oxides with very steep gradients, decreasing to near zero concentrations within the first centimeter of the sediment. This more likely indicates low rates of Mn oxide reduction, rather than rapid reduction rates. For instance, the slow OM deposition rates that are characteristic of deep-sea environments allows for Mn oxides at

the sediment surface to continually oxidize Mn in seawater, increasing surface concentrations (Burdige 2006). Additionally, the benthic remobilization of Mn into the water column has been well correlated with high rates of OM deposition and subsequent decreases in pore-water oxygen penetration depth (Aller 1994b). Thus, the more oxic conditions of the off-shelf region may allow for the retention of reduced Mn in the sediment (Burdige 2006). The relatively high rates of Mn reduction in the off-shelf region may also be overestimates. The diffusive model likely overestimates bioturbation rates in this region, which would lead to the overestimation of the depth-integrated rate of metal reduction (Eq.6).

Nonetheless, Mn reduction rates were low in all regions and the lack of any significant correlation between rates of sediment oxygen uptake and Mn reduction rates (Fig. 12) can be explained by the minor role of Mn oxide reduction found in the southeast Bering Sea. This is similar to patterns found by both Kostka et al. (1999) and Nickel et al. (2008), where Mn oxide reduction was negligible in Arctic and Barents Sea sediments.

4.3 Estimations of Total Carbon Oxidation Rates

It is important to address assumptions made regarding the calculation of the fraction of OM remineralized via the reduction of these metal oxides. Total oxygen consumption was used as a proxy for total OM remineralization under the assumption that all oxygen consumed is either directly or indirectly linked to carbon mineralization (i.e.: aerobic respiration or reoxidizing other terminal electron acceptors). It has been shown that in deep sea pelagic sediments below 1000 m (as in the off-shelf region), aerobic respiration is the dominate pathway for OM remineralization (Archer et al. 2002, Burdige 2006).

However, as water depths decrease and OM flux to the sediments increases, pore-water oxygen can be depleted before all OM is remineralized (Emerson and Hedges 2003). In this case, total oxygen uptake may not necessarily be used for aerobic respiration, but rather for the oxidation of other reduced compounds, like Fe^{2+} and Mn^{2+}. If these complex interactions between the respiratory pathways in the sediments are tightly coupled and all reduced end-products of anaerobic pathways are oxidized, then total oxygen consumption rates can still be a good estimate of total sediment respiration rates. However, if sedimentary respiration pathways become de-coupled, as may occur under non-steady-state conditions, oxygen consumption rates can underestimate total OM oxidation if reduced end-products are stored at depth, such as iron sulfides (Burdige 2006). On the other hand, rates of oxygen uptake may overestimate carbon oxidation if stored compounds are oxidized. Nonetheless, here I assumed a complete coupling of aerobic and anaerobic respiratory pathways and interpreted oxygen consumption rates as a suitable measure of total OM remineralization.

5.0 Conclusions

The reduction of Fe oxides was found to be an important pathway of carbon oxidation in the southeastern Bering Sea, whereas Mn reduction was determined to be of minor importance. Further investigation of the patterns of Fe reduction, however, could be helpful in order to better understand factors influencing both Fe reduction rates and primary production in this region.

The highest ratios of Fe reduction to total carbon oxidation were found in the northern and middle regions of the Bering Sea, which have been noted as having Fe-replete surface waters (Aguilar-Islas et al. 2007, Hurst et al. 2010). Given the relatively high rates of Fe reduction in this region and the extremely low percentage of reduced Fe that would need to escape the sediment to support primary production, it may be that sedimentary reduction of Fe oxides is a significant source of leachable, particulate Fe to surface waters. Therefore, by possibly supplying a significant fraction of Fe available to the water column, sedimentary Fe reduction may play an important role in regulating primary production in the southeastern Bering Sea.

6.0 Literature Cited

Aguilar-Islas, A.M., M.P. Hurst, K.N. Buck, B. Sohst, G.J. Smith, M.C. Lohan and K.W. Bruland, 2007. Micro- and macronutrients in the southeastern Bering Sea: Insight into the iron-replete and iron-depleted regimes. Prog. Ocean. 73: 99-126.

Aller, R.C. 1990. Bioturbation and manganese cycling in hemipelagic sediments. Phil. Trans. R. Soc. London, A. 331: 51-68.

Aller, R.C. 1994a. Bioturbation and remineralization of sedimentary organic matter: effects of redox oscillation. Chem. Geol. 114: 331-345.

Aller, R.C., 1994b. The sedimentary Mn cycle in Long Island Sound: its role as intermediate oxidant and the influence of bioturbation, O_2, and C_{org}, flux on diagenetic reaction balances. J. Mar. Res. 52: 259-295.

Aller, R.C and J.K Cochran 1976. $^{234}Th/^{238}U$ disequilibrium in near-shore sediment: particle reworking and diagenetic time scales. Earth Planet. Sci. Lett. 29: 37-50.

Archer, D.E., J.L. Morford and S.R. Emerson, 2002. A model of suboxic sedimentary diagenesis suitable for automatic tuning and gridded global domains. Global Biogeochem. Cycles 16: 10.1029/2000GB001288.

Berg P, Rysgaard S, Thamdrup B. 2003. Dynamic modeling of early diagenesis and nutrient cycling: a case study in an arctic marine sediment. Am. J. Sci. 303: 905–955.

Brand, L.E. 1991. Minimum iron requirements for marine phytoplankton and the Implications for the biogeochemical control of new production. Limnol. Oceanogr. 36: 1756-1771.

Burdige, D.J. 1993. The biogeochemistry of managanese and iron reduction in marine sediments. Earth-Sci. Rev. 35: 249-284.

Burdige, D.J. 2006. Geochemistry of marine sediments. Princeton University Press, Princeton, New Jersey, 609.

Bruland, K.W. and M.C. Lohan, 2003. Controls of trace metals in seawater. In *The Oceans and Marine Geochemistry* (ed. H. Elderfield) Vol. 6 *Treatise on Geochemistry* (eds. H.D. Holland and K.K Turekian), Elsevier, pp. 23-47.

Canfield, D.E., B.B. Jorgensen, H. Fossing, R. Glud, J. Gunderson, N.B. Ramsing, B. Thamdrup, J.W. Hansen, L.P Nielson and P.O.J. Hall, 1993a. Pathways of organic Carbon oxidation in three continental margin sediments. Mar. Geol. 113: 27-40.

Canfield, D.E., B. Thamdrup and J.W. Hansen, 1993b. The anaerobic degradation of organic matter in Danish coastal sediments: Iron reduction, manganese reduction, and sulfate reduction. Geochim. Cosmochim. Acta. 57:3867-3883.

Cooper, L.W., J.M. Grebmeier, I.L. Larsen, V.G. Egorov, C. Theodorakis, H.P. Kelly and J.R. Lovvorn, 2002. Seasonal variation in sedimentation of organic materials in the St. Lawrence Island polynya region, Bering Sea. Mar. Ecol. Prog. Ser. 226: 13-26.

Coyle, K.O., B. Konar, A. Blanchard, R.C. Highsmith, J. Carroll, M. Carroll, S.G. Denisenko and B.I. Sirenko, 2007. Potential effects of temperature on the benthic infaunal community of the southeastern Bering Sea shelf: Possible impacts of climate change. Deep-Sea Res. 54: 2885-2905.

Davenport, E.S., 2008. Phosphate cycling in Bering Sea sediments. Master's thesis, Western Washington University.

Dauwe, B., P.M.J. Herman and C.H.R. Heip, 1998. Community structure and bioturbation potential at four North Sea stations with contrasting food supply. Mar. Ecol. Prog. Ser. 173: 67-83.

Emerson, S. and J. Hedges 2003. Sediment diagenesis and benthic flux. In *Sediments, Diagenesis, and Sedimentary Rocks* (ed. F.T. Mackenzie) Vol. 6 *Treatise on Geochemistry* (eds. H.D. Holland and K.K. Turekian). Elsevier, pp 293-319.

Froelich, P.N., G.P. Klinkhammer, M.L. Bender, N.A. Luedtke, G.R. Heath, D. Cullen, P. Dauphin, D. Hammond, B. Hartman and V. Maynard, 1979. Early oxidation of organic matter in pelagic sediments of the eastern equatorial Atlantic: suboxic diagenesis. Geochim. Cosmochim. Acta 43: 1075-1090.

Giblin, A.E., C.S. Hopkinson and J. Tucker, 1997. Benthic metabolism and nutrient cycling in Boston Harbor, Massachusetts. Estuaries 20: 346-364.

Gordon, L. I., J. C. Jennings, Jr., A. A. Ross, and J. M. Krest. 1994. A suggested protocol for continuous flow automated analysis of seawater nutrients (phosphate, nitrate, nitrite and silicic acid) in the WOCE Hydrographic Program and the Joint Global Ocean Fluxes Study. In WOCE Operations Manual. WHP Office Report WHPO 91-1. WOCE Report No. 68/91. Revision 1. Woods Hole, Mass.

Glud, R.N., N. Risgaard-Peterson, B. Thamdrup, H. Fossing and S. Rysgaard, 2000. Benthic carbon mineralization in a high-Arctic sound (Young Sound, NE Greenland). Mar. Ecol. Prog. Ser. 206: 59-71.

Grebmeier, J.M., C.P. McRoy and H.M Feder, 1988. pelagic-benthic coupling on the shelf of the northern Bering and Chuckchi seas. I. Food supply source and benthic biomass. Mar. Ecol. Prog. Ser. 48: 57-67.

Grebmeier, J.M., H.M. Feder and C.P. McRoy, 1989. Pelagic-benthic coupling on the Shelf of the northern Bering and Chukchi Seas. II. Benthic community structure. Mar. Ecol. Prog. Ser. 51: 253-268.

Grebmeier, J.M., J.E. Overland, S.E. Moore, E.V. Farley, E.C. Carmack, L.W. Cooper, K.E. Frey, J.H. Helle, F.A. McLaughlin and S.L McNutt 2006. A major ecosystem shift in the northern Bering Sea. Science 311: 1461-1464.

Hollander, M. and D. A. Wolfe. 1973. Nonparametric Statistical Methods, Wiley, 526 pp.

Hood, D.W., 1981. Introduction. In *The Eastern Bering Sea Shelf: Oceanography and Resources* Vol. 1 (eds. D.W. hood and J.A. Calder). Univ. of Washington, pp. xiii-xviii.

Hulth, S., R.C. Aller and F. Gilbert, 1999. Coupled anoxic nitrification/manganese Reduction in marine sediments. Geochim. Cosmochim. Acta 63: 49-66.

Hunt, G.L., P. Stabeno, G. Walters, E. Sinclair, R.D. Brodeur, J.M. Napp and N.A. Bond, 2002. Climate change and control of the southeastern Bering Sea pelagic ecosystem. Deep-Sea Res. (II) 49: 5821-5853.

Hurst, M.P., A.M. Aguilar-Islas and K.W. Bruland, 2010. Iron in the southeastern Bering Sea: Elevated leachable particulate Fe in shelf bottom waters as an important source for surface waters. Cont. Shelf Res. 30: 467-480.

Jensen, M.M., B. Thamdrup, S. Rysgaard, M. Holmer and H. Fossing, 2003. Rates and regulation of microbial iron reduction in sediments of the Baltic-North Sea transition. Biogeochemistry 65: 295-317.

Kostka, J.E., E. Haefele, R. Viehweger and J.W. Stucki, 1999. Respiration and dissolution of iron(III)-containing clay minerals by bacteria. Environ. Sci. Technol. 33: 3127-3133.

Kostka, J.E., B. Gribsholt, E. Petrie, D. Dalton, H. Skelton and E. Kristensen, 2002. The rates and pathways of carbon oxidation in bioturbated saltmarsh sediments. Limnol. Oceanogr. 47: 230-240.

Lecroart, P. M. Olivier, S. Schmidt, A. Grémare, P. Anschutz and J.R.F. Meysman, 2010. Bioturbation, short-lived radioisotopes, and the tracer-dependence of biodiffusion coefficients. Geochim. Cosmochim. Acta 21: 6049-6063.

Lovely, D.R., 1991. Dissimilatory Fe(III) and Mn(IV) Reduction. Microb. Rev. 55: 259-287.

Lovvorn, J.R., L.W. Cooper, M.L. Brooks, C.C. De Ruyck, J.K. Bump and J.M. Grebmeier, 2005. Organic matter pathways to zooplankton and benthos under pack ice in late winter and open water in late summer in the north-central Bering Sea. Mar. Ecol. Prog. Ser. 291:135-150.

Marinelli, R.A., R.A. Jahnke, D.B. Craven, J.R. Nelson and J.E. Eckman, 1998. Sediment nutrient dynamics on the South Atlantic Bight Continental Shelf. Limnol. Oceanogr. 43: 1305-1320.

Martin, W.R. and F.L. Sayles 2003. The recycling of biogenic material at the seafloor. In *Sediments,Diagenesis, and Sedimentary Rocks* (ed. F.T. Mackenzie) Vol. 6 *Treatise on Geochemistry* (eds. H.D. Holland and K.K. Turekian). Elsevier, pp. *37-65.*

Meysman, F.J.R., B.P. Boudreau and J.J. Middelburg, 2003. Relations between local, nonlocal, discrete and continuous models of bioturbation. J. Mar. Res. 61: 391-410.

Moore, J.K., S.C. Doney, D.M. Glover and I.Y. Fung, 2002. Iron cycling and nutrient-limitation patterns in surface waters of the world ocean. Deep-Sea Res. (II) 49: 463-507.

Nickel, M., V. Vandieken, V. Brüchert and B.B. Jørgensen, 2008. Microbial Mn(IV) and Fe(III) reduction in northern Barents Sea sediments under different conditions of ice cover and organic carbon deposition. Deep-Sea Res. (II) 55: 2390-2398.

Phillips, E.J.P. and D.R. Lovely 1987. Determination of Fe(III) and Fe(II) in oxalate extracts of sediment. Soil Sci. Am. J. 51: 938-941.

Revsbech, N.P. 1989. An oxygen microsensor with a guard cathode. Limnol. Oceanogra. 34: 474-478.

Richter, R. 1952. Sediment-Gaseinien und Sedifluktion uberhaupt: Notizbl. Hess. L.-Amt. Bodenforsch 3: 67-81.

Robbins, J.M., M. Lyle and G.R. Heath, 1984. A sequential extraction procedure for partioning elements among co-exisiting phases in marine sediments. College of Oceanography, Oregon State Univ. Ref. 84-3, 64 pp.

Smith, C.R., R.H. Pope, D.J. DeMaster and L. Magaard, 1993. Age-dependent mixing of deep-sea sediments. Geochim. Cosmochim. Acta 57: 1473-1488.

Springer, A.M., C.P. McRoy and M.V. Flint, 1996. The Bering Sea Green Belt: Shelf-edge processes and ecosystem production. Fisheries Oceanogra. 5: 205-223.

Stabeno, P.J. and G.L. Hunt, 2002. Overview of the Inner front and Southeast Bering Sea carrying capacity programs. Deep-Sea Res. (II) 49: 6157-6168.

Stabeno, P.J., N.A. Bond, N.B. Kachel, S.A. Salo and J.D. Schumacher, 2001. On the temporal variability of the physical environment over the south-eastern Bering Sea. Fisheries Oceanography 10: 81-98.

Thamdrup, B., 2000. Bacterial manganese and iron reduction in aquatic sediments. In *Advances in Microbial Ecology* Vol. 6 (ed. B. Schink). Kluwer Academic, pp. 41-84.

Thamdrup, B. and D.E. Canfield, 1996. Pathways of carbon oxidation in continental margin sediments off central Chile. Limnol. Oceanogr. 41: 1629-1650.

Thamdrup, B., R. Rossello-Mora and R. Amann, 2000. Microbial manganese and sulfate reduction in Black sea shelf sediments. Appl. Environ. Microbiol. 66: 2888-2897.

Vandieken, V., M. Nickel and B.B. Jørgensen, 2006. Carbon mineralization in Arctic Sediments northeast of Svalbard: Mn(IV) and Fe(III) as principal anaerobic Respiratory pathways. Mar. Ecol. Prog. Ser. 322: 15-27.

Walsh, J.J. and C.P. McRoy, 1986. Ecosystem analysis in the southeastern Bering Sea. Cont. Shelf Res. 5: 259-288.

Wang, Y. and P. Van Cappellen, 1996. A multicomponent reactive transport model of early diagenesis: application to redox cyxling in coastal marine sediments. Geochim. Cosmochim. Acta. 60: 2993-3014.

Wijsman, J.W.M., J.J. Middleburg and C.H.R. Heip, 2001. Reactive iron in Black Sea Sediments: implications for iron cycling. Mar. Geol. 172: 167-180.

7.0 Appendix. Summary table showing porosity values, excess ^{234}Th profiles, solid-phase and pore-water Fe and Mn profiles. Pore-water profiles for stations marked with (†) represent average values from duplicate cores.

Station	Avg. Depth (cm)	Porosity	Excess Th-234 (dpm g^{-1})	Fe concentration (umoles g^{-1})	Mn concentration (umoles g^{-1})	Pore water Fe (uM)	Pore water Mn (uM)
HLY 9	0.25	0.71	5.88 (± 0.46)	143.07	2.58	-	-
	0.75	0.58	0.50 (± 0.19)	138.29	0.93	-	-
	1.25	0.61	-0.56 (± 0.14)	106.46	0.62	-	-
	1.75	0.61	0.70 (± 0.23)	85.99	0.58	-	-
	2.5	0.63	-	86.54	0.53	-	-
	3.5	0.63	-	84.50	0.67	-	-
	5.5	0.57	-	88.94	0.58	-	-
	7.5	0.55	-	81.14	0.56	-	-
	9.5	0.44	-	67.45	0.55	-	-
†HLY 17	0.25	0.87	22.07 (± 1.87)	170.04	2.37	3.87	0.62
	0.75	0.78	4.94 (± 0.52)	213.93	1.58	3.45	1.53
	1.25	0.76	-0.40 (± 0.20)	161.55	1.06	34.93	3.64
	1.75	0.76	-	138.60	1.04	62.96	4.05
	2.5	0.76	-	152.33	1.04	71.52	4.73
	3.5	0.73	-	136.32	1.16	75.83	3.75
	5.5	0.75	-	130.58	1.15	59.19	3.17
	7.5	0.70	-	114.14	1.00	54.26	2.03
	9.5	0.72	-	127.41	1.16	45.62	2.01
†HLY 19	0.25	0.81	5.07 (± 0.63)	111.29	1.07	3.05	0.25
	0.75	0.76	1.43 (± 0.28)	118.74	0.89	4.26	0.95
	1.25	0.74	1.53 (± 0.33)	113.47	0.96	9.43	1.48
	1.75	0.75	-	99.54	0.91	20.55	1.84
	2.5	0.75	-	92.45	0.80	39.10	2.05
	3.5	0.75	-	90.46	0.82	45.85	1.83
	5.5	0.73	-	85.22	0.62	33.21	1.53
	7.5	0.71	-	96.34	0.66	65.23	1.37
	9.5	0.71	-	72.68	0.67	27.01	1.27
HLY 25	0.25	0.82	8.48 (± 0.77)	76.01	0.75	3.88	0.63
	0.75	0.78	1.13 (± 0.28)	71.50	0.66	4.76	0.78
	1.25	0.80	-	55.35	0.56	10.02	0.90
	1.75	0.76	-	53.18	0.58	9.50	0.89
	2.5	0.74	-	52.74	0.56	9.94	0.79
	3.5	0.72	-	58.16	0.60	5.63	0.77
	5.5	0.72	-	53.52	0.42	4.12	0.27
	7.5	0.72	-	44.89	0.47	5.38	0.37
	9.5	0.72	-	46.18	0.55	2.09	0.00
†HLY 26	0.25	0.69	13.66 (± 0.84)	81.74	5.35	3.79	0.71
	0.75	0.69	0.62 (± 0.17)	96.44	4.42	3.83	0.79
	1.25	0.67	0.45 (± 0.13)	64.75	0.75	3.15	0.53
	1.75	0.66	-	61.44	0.75	3.81	0.96
	2.5	0.63	-	58.68	0.67	1.94	0.24
	3.5	0.64	-	76.35	0.75	7.42	0.70
	5.5	0.64	-	82.83	0.89	19.26	1.05
	7.5	0.64	-	91.21	0.91	20.56	2.46
	9.5	0.64	-	89.89	1.00	7.99	0.18

Appendix cont.

Station	Avg. Depth (cm)	Porosity	Excess Th-234 (dpm g^{-1})	Fe concentration (umoles g^{-1})	Mn concentration (umoles g^{-1})	Pore water Fe (uM)	Pore water Mn (uM)
†HLY 32	0.25	0.79	15.43 (± 0.10)	166.79	1.97	3.81	3.67
	0.75	0.84	2.72 (± 0.13)	220.53	5.61	92.39	10.76
	1.25	0.81	2.01 (± 0.10)	245.26	2.00	94.44	8.28
	1.75	0.77	1.29 (± 0.09)	150.14	0.73	113.04	7.18
	2.5	0.74	-	158.20	0.84	129.68	6.62
	3.5	0.71	-	126.65	0.73	134.73	5.57
	5.5	0.67	-	106.29	0.75	72.49	5.01
	7.5	0.61	-	85.91	0.60	37.63	6.89
	9.5	0.62	-	89.03	0.51	38.91	5.80
†HLY 35	0.25	0.72	5.00 (± 0.46)	102.74	1.97	5.64	0.90
	0.75	0.64	1.62 (± 0.28)	101.35	1.80	4.29	3.65
	1.25	0.62	0.80 (± 0.16)	106.88	1.22	5.02	5.27
	1.75	0.59	1.25 (± 0.20)	116.19	2.15	3.50	6.89
	2.5	0.53	-	108.64	0.82	9.49	9.17
	3.5	0.56	-	95.92	0.60	15.26	7.54
	5.5	0.55	-	109.32	0.40	59.34	3.68
	7.5	0.51	-	68.03	0.40	-	-
	9.5	0.52	-	55.76	0.42	-	-
†HLY 39	0.25	0.68	6.04 (± 0.56)	92.56	2.69	4.27	1.51
	0.75	0.66	3.21 (± 0.42)	109.41	1.27	8.55	11.39
	1.25	0.66	1.55 (± 0.24)	113.61	1.82	35.70	20.02
	1.75	0.67	0.90 (± 0.20)	96.75	0.87	46.05	30.18
	2.5	0.68	-	91.95	0.84	61.36	27.38
	3.5	0.68	-	107.26	0.73	87.51	24.09
	5.5	0.66	-	80.97	0.62	183.34	13.66
	7.5	0.62	-	65.77	0.56	191.76	9.28
	9.5	0.59	-	69.15	0.51	-	-
HLY 54	0.25	0.73	10.56 (± 0.92)	120.22	1.86	-	-
	0.75	0.57	1.16 (± 0.20)	94.97	0.96	-	-
	1.25	0.55	0.51 (± 0.06)	92.91	0.64	-	-
	1.75	0.54	-	64.39	0.51	-	-
	2.5	0.51	-	55.80	0.56	-	-
	3.5	0.51	-	51.25	0.47	-	-
	5.5	0.50	-	64.23	0.49	-	-
	7.5	0.46	-	54.49	0.31	-	-
	9.5	0.47	-	48.74	0.53	-	-
HLY 58	0.25	0.66	3.43 (± 0.39)	73.52	0.89	-	-
	0.75	0.64	0.35 (± 0.14)	78.05	0.98	-	-
	1.25	0.50	0.85 (± 0.18)	58.02	0.56	-	-
	1.75	0.45	-	65.05	0.66	-	-
	2.5	0.46	-	55.88	0.62	-	-
	3.5	0.48	-	59.97	0.42	-	-
	5.5	0.41	-	50.96	0.31	-	-
	7.5	0.40	-	42.04	0.29	-	-
	9.5	0.41	-	44.93	0.36	-	-

Appendix cont.

Station	Avg. Depth (cm)	Porosity	Excess Th-234 (dpm g^{-1})	Fe concentration (umoles g^{-1})	Mn concentration (umoles g^{-1})	Pore water Fe (uM)	Pore water Mn (uM)
†HLY 65	0.25	0.78	35.94 (± 1.81)	81.78	0.89	3.09	0.49
	0.75	0.72	9.88 (± 0.86)	78.82	0.49	3.35	0.71
	1.25	0.64	3.50 (± 0.48)	58.70	0.47	3.71	1.00
	1.75	0.63	1.30 (± 0.22)	60.88	0.53	7.39	1.36
	2.5	0.65	-	56.42	0.53	7.73	0.93
	3.5	0.62	-	55.94	0.47	17.66	0.75
	5.5	0.61	-	44.64	0.40	-	-
	7.5	0.64	-	43.92	0.29	-	-
	9.5	0.64	-	42.76	0.29	-	-
HLY 69	0.25	0.82	21.87 (± 1.92)	139.52	1.49	4.17	0.77
	0.75	0.78	7.28 (± 0.88)	128.35	0.75	4.06	1.44
	1.25	0.76	3.41 (± 0.49)	79.52	0.62	6.13	1.41
	1.75	0.74	-	75.98	0.67	31.98	1.46
	2.5	0.73	-	77.52	0.60	40.07	1.47
	3.5	0.73	-	74.85	0.64	59.85	1.37
	5.5	0.70	-	72.39	0.64	41.59	1.25
	7.5	0.67	-	63.51	0.67	25.16	0.84
	9.5	0.65	-	68.31	0.69	10.87	0.43
HLY 73	0.25	0.80	13.57 (± 1.02)	103.27	1.16	4.39	1.14
	0.75	0.77	0.91 (± 0.28)	100.42	1.04	5.37	2.43
	1.25	0.74	0.85 (± 0.28)	73.01	0.75	22.26	4.36
	1.75	0.73	-	66.20	0.71	16.51	4.20
	2.5	0.73	-	73.38	0.86	22.23	3.36
	3.5	0.72	-	76.32	0.73	50.79	1.72
	5.5	0.69	-	76.91	0.78	33.02	1.32
	7.5	0.67	-	64.39	0.75	33.17	1.09
	9.5	0.67	-	65.93	0.76	-	-
HLY 83	0.25	0.87	23.33 (± 1.91)	195.54	3.04	3.79	0.93
	0.75	0.81	6.57 (± 0.50)	163.56	1.16	7.91	3.04
	1.25	0.82	2.42 (± 0.31)	132.21	1.04	36.59	2.79
	1.75	0.80	-	129.47	1.07	71.13	3.22
	2.5	0.80	-	157.88	1.07	71.62	3.50
	3.5	0.80	-	150.15	1.06	71.62	3.75
	5.5	0.78	-	145.53	1.11	62.61	3.28
	7.5	0.76	-	150.42	1.06	66.00	3.22
	9.5	0.74	-	131.29	1.07	48.55	2.77
HLY 90	0.25	0.78	11.76(± 0.78)	105.74	1.06	4.36	0.68
	0.75	0.77	1.52 (± 0.33)	117.45	0.78	2.98	0.95
	1.25	0.77	-0.33 (± 0.18)	90.84	0.66	5.64	1.42
	1.75	0.75	-	72.15	0.66	15.22	1.43
	2.5	0.71	-	66.04	0.67	19.02	1.73
	3.5	0.71	-	63.62	0.67	16.22	1.05
	5.5	0.68	-	63.80	0.69	13.65	1.07
	7.5	0.68	-	68.14	0.67	24.52	0.62
	9.5	0.67	-	74.01	0.80	24.28	0.00

Appendix cont.

Station	Avg. Depth (cm)	Porosity	Excess Th-234 (dpm g^{-1})	Fe concentration (umoles g^{-1})	Mn concentration (umoles g^{-1})	Pore water Fe (uM)	Pore water Mn (uM)
HLY 92	0.25	0.83	19.41 (± 1.41)	193.02	3.64	3.01	1.05
	0.75	0.83	7.68 (± 0.81)	175.47	1.89	10.49	9.55
	1.25	0.78	4.99 (± 0.63)	121.93	0.84	52.96	5.38
	1.75	0.79	-	106.17	0.71	65.52	3.86
	2.5	0.77	-	115.36	0.67	91.32	3.00
	3.5	0.76	-	107.08	0.66	97.16	2.45
	5.5	0.68	-	94.57	0.64	71.19	1.88
	7.5	0.66	-	85.68	0.56	44.68	1.46
	9.5	0.63	-	94.85	0.62	40.93	1.09
HLY 93	0.25	0.74	4.46 (± 0.52)	104.74	1.64	0.00	3.89
	0.75	0.63	2.05 (± 0.40)	101.82	0.86	90.67	13.07
	1.25	0.61	1.09 (± 0.30)	111.06	1.07	102.25	10.25
	1.75	0.61	-	102.66	0.95	118.45	9.04
	2.5	0.62	-	103.86	0.86	156.88	7.06
	3.5	0.61	-	90.50	0.75	130.78	7.94
	5.5	0.57	-	99.11	0.87	157.92	8.80
	7.5	0.54	-	61.15	0.60	111.90	4.03
	9.5	0.55	-	56.53	0.56	0.00	1.47
†HLY 98	0.25	0.87	32.06 (± 1.71)	159.21	1.89	2.07	0.69
	0.75	0.84	4.58 (± 0.65)	175.52	1.47	2.29	3.31
	1.25	0.79	2.46 (± 0.46)	168.95	0.91	22.44	3.77
	1.75	0.76	-	128.23	0.71	47.13	1.99
	2.5	0.75	-	98.74	0.55	69.72	1.57
	3.5	0.73	-	96.48	0.73	77.27	1.82
	5.5	0.69	-	86.83	0.56	71.05	1.94
	7.5	0.68	-	79.02	0.56	60.73	1.69
	9.5	0.65	-	106.97	0.47	34.93	1.01
†HLY 116	0.25	0.79	15.78 (± 1.25)	119.63	0.86	4.65	0.61
	0.75	0.75	1.66 (± 0.35)	123.22	0.76	5.14	1.25
	1.25	0.74	2.30 (± 0.42)	81.24	0.47	8.23	1.48
	1.75	0.72	-	85.54	0.44	16.68	1.46
	2.5	0.56	-	88.12	0.49	19.88	1.14
	3.5	0.72	-	85.86	0.56	27.51	1.16
	5.5	0.68	-	100.85	0.47	10.79	0.48
	7.5	0.69	-	77.00	0.55	18.73	0.22
	9.5	0.68	-	74.85	0.47	16.70	0.31
†KNR 1	0.25	0.895	44.51 (± 3.35)	126.49	1.69	3.72	1.01
	0.75	0.905	10.77 (± 0.89)	120.48	1.58	3.59	1.01
	1.25	0.898	2.40 (± 0.40)	130.77	1.11	3.49	1.02
	1.75	0.879	-	120.73	1.07	3.65	1.05
	2.5	0.869	-	116.81	1.04	4.08	1.16
	3.5	0.855	-	109.97	1.04	3.59	1.11
	5.5	0.833	-	97.70	0.96	3.75	1.09
	7.5	0.833	-	101.39	0.98	4.96	1.44
	9.5	0.822	-	102.50	0.98	8.01	2.06

Appendix cont.

Station	Avg. Depth (cm)	Porosity	Excess Th-234 (dpm g^{-1})	Fe concentration (umoles g^{-1})	Mn concentration (umoles g^{-1})	Pore water Fe (uM)	Pore water Mn (uM)
KNR 17	0.25	0.496	2.94 (± 0.34)	58.91	0.95	-	-
	0.75	0.472	1.10 (± 0.12)	64.25	0.42	-	-
	1.25	0.447	0.35 (± 0.13)	71.93	0.42	-	-
	1.75	0.423	-	66.29	0.31	-	-
	2.5	0.435	-	68.31	0.25	-	-
	3.5	0.444	-	48.65	0.20	-	-
	5.5	0.458	-	41.83	0.16	-	-
	7.5	0.467	-	44.71	0.22	-	-
	9.5	0.461	-	33.66	0.16	-	-
†KNR 22	0.25	0.861	13.15 (± 0.86)	111.02	1.06	3.41	4.64
	0.75	0.795	2.10 (± 0.29)	114.85	0.89	3.43	5.44
	1.25	0.778	2.05 (± 0.36)	101.69	0.76	2.40	3.05
	1.75	0.729	-	101.44	0.78	3.45	3.09
	2.5	0.709	-	81.44	0.66	11.33	3.01
	3.5	0.705	-	74.60	0.64	16.44	1.98
	5.5	0.662	-	68.40	0.47	6.48	1.38
	7.5	0.617	-	68.91	0.55	8.44	1.42
	9.5	0.626	-	80.51	0.64	5.58	1.61
†KNR 27	0.25	0.955	102.94 (± 7.87)	111.31	17.53	4.51	1.00
	0.75	0.922	9.01 (± 0.86)	115.44	6.53	3.91	1.23
	1.25	0.914	0.44 (± 0.30)	104.56	1.66	4.10	1.83
	1.75	0.917	-	132.96	4.48	3.99	2.33
	2.5	0.917	-	62.71	0.44	4.17	2.64
	3.5	0.912	-	58.77	0.46	6.22	2.84
	5.5	0.901	-	67.40	0.49	4.26	2.93
	7.5	0.893	-	61.06	0.53	4.11	3.34
	9.5	0.878	-	65.95	0.51	5.39	2.85
KNR 32	0.25	0.708	5.51 (± 0.54)	83.84	1.75	-	-
	0.75	0.546	1.04 (± 0.25)	84.27	1.05	-	-
	1.25	0.560	1.03 (± 0.21)	89.65	0.35	-	-
	1.75	0.534	-	81.91	0.23	-	-
	2.5	0.533	-	62.96	0.14	-	-
	3.5	0.547	-	57.87	0.23	-	-
	5.5	0.545	-	55.56	0.20	-	-
	7.5	0.529	-	56.77	0.40	-	-
	9.5	0.514	-	64.42	0.47	-	-
KNR 45	0.25	0.719	4.85 (± 0.37)	89.64	1.18	-	-
	0.75	0.548	0.92 (± 0.15)	85.81	0.80	-	-
	1.25	0.454	0.50 (± 0.15)	85.34	0.25	-	-
	1.75	0.451	-	76.94	0.05	-	-
	2.5	0.451	-	57.05	0.01	-	-
	3.5	0.464	-	46.30	0.03	-	-
	5.5	0.435	-	37.29	0.00	-	-
	7.5	0.412	-	39.00	0.02	-	-
	9.5	0.410	-	34.71	0.01	-	-

Appendix cont.

Station	Avg. Depth (cm)	Porosity	Excess Th-234 (dpm g^{-1})	Fe concentration (umoles g^{-1})	Mn concentration (umoles g^{-1})	Pore water Fe (uM)	Pore water Mn (uM)
†KNR 53	0.25	0.953	63.91 (± 4.84)	156.30	16.83	3.50	0.74
	0.75	0.938	5.01 (± 1.20)	222.96	8.98	3.39	0.84
	1.25	0.933	14.53 (± 0.85)	242.52	1.87	3.44	1.56
	1.75	0.908	-	119.88	0.74	4.05	2.40
	2.5	0.924	-	90.70	0.52	3.59	3.72
	3.5	0.912	-	85.84	0.60	3.95	4.21
	5.5	0.902	-	74.34	0.51	3.79	5.47
	7.5	0.898	-	69.38	0.57	3.63	5.84
	9.5	0.889	-	70.82	0.69	3.88	5.84
KNR 60	0.25	0.523	4.11 (± 0.40)	29.37	0.17	-	-
	0.75	0.482	0.06 (± 0.19)	32.67	0.00	-	-
	1.25	0.462	-0.53 (± 0.13)	31.96	0.00	-	-
	1.75	0.444	-	39.03	0.00	-	-
	2.5	0.446	-	33.91	0.00	-	-
	3.5	0.431	-	30.62	0.00	-	-
	5.5	0.448	-	27.87	0.00	-	-
	7.5		-	28.93	0.00	-	-
	9.5		-		0.00	-	-
†KNR 67	0.25	0.923	23.82 (± 1.86)	106.61	28.57	3.86	0.67
	0.75	0.912	1.32 (± 0.59)	98.41	20.17	3.32	0.69
	1.25	0.907	-0.30 (± 0.53)	100.46	1.45	3.34	0.80
	1.75	0.906	-	66.14	0.88	3.42	2.80
	2.5	0.893	-	64.85	0.96	3.92	5.09
	3.5	0.886	-	72.90	1.06	3.66	7.08
	5.5	0.871	-	65.69	1.35	4.63	9.22
	7.5	0.869	-	48.71	1.16	9.12	10.96
	9.5	0.871	-	52.66	1.28	3.60	11.45
KNR 79	0.25	0.775	18.12 (± 1.27)	62.85	1.18	3.34	0.70
	0.75	0.687	2.78 (± 0.28)	65.94	0.86	3.25	0.95
	1.25	0.592	1.03 (± 0.20)	69.62	0.52	3.49	1.34
	1.75	0.586	-	54.65	0.38	91.35	4.32
	2.5	0.593	-	51.65	0.42	12.99	2.46
	3.5	0.592	-	37.03	0.32	7.86	1.73
	5.5	0.541	-	32.69	0.25	-	-
	7.5	0.545	-	35.67	0.27	-	-
	9.5	0.572	-	40.74	0.39	-	-
KNR 89	0.25	0.724	18.15 (± 1.37)	163.02	2.97	3.32	1.02
	0.75	0.608	5.72 (± 0.61)	158.53	1.08	7.64	4.87
	1.25	0.660	2.00 (± 0.24)	141.24	1.02	30.11	5.27
	1.75	0.604	-	142.60	0.99	35.49	4.72
	2.5	0.622	-	142.90	0.88	57.39	4.84
	3.5	0.613	-	119.20	0.80	47.77	4.31
	5.5	0.530	-	102.98	0.76	38.75	4.71
	7.5	0.559	-	103.87	0.71	12.58	2.83
	9.5	0.549	-	103.94	0.71	13.19	2.87

Appendix cont.

Station	Avg. Depth (cm)	Porosity	Excess Th-234 (dpm g^{-1})	Fe concentration (umoles g^{-1})	Mn concentration (umoles g^{-1})	Pore water Fe (uM)	Pore water Mn (uM)
KNR 106	0.25	0.854	5.80 (± 0.51)	143.32	1.53	4.53	1.63
	0.75	0.833	1.86 (± 0.29)	139.49	1.52	5.77	4.20
	1.25	0.783	-0.56 (± 0.29)	145.77	1.40	-	-
	1.75	0.783	-	132.40	1.19	-	-
	2.5	0.728	-	133.99	1.18	23.25	3.58
	3.5	0.742	-	131.81	1.21	40.97	3.51
	5.5	0.731	-	104.08	0.97	36.66	3.53
	7.5	0.721	-	107.68	0.98	22.41	2.51
	9.5	0.719	-	120.91	1.12	14.08	2.43
KNR 113	0.25	0.691	9.40 (± 0.71)	56.10	0.67	-	-
	0.75	0.649	1.83 (± 0.28)	65.00	0.69	-	-
	1.25	0.627	0.74 (± 0.36)	58.18	0.53	-	-
	1.75	0.610	-	46.92	0.46	-	-
	2.5	0.600	-	38.54	0.49	-	-
	3.5	0.555	-	38.70	0.46	-	-
	5.5	0.562	-	40.81	0.46	-	-
	7.5	0.557	-	37.44	0.56	-	-
	9.5	0.541	-	41.76	0.55	-	-
KNR 115	0.25	-	-	71.16	1.07	-	-
	0.75	-	-	79.76	1.06	-	-
	1.25	-	-	72.40	1.16	-	-
	1.75	-	-	85.76	1.57	-	-
	2.5	-	-	90.21	0.71	-	-
	3.5	-	-	89.57	0.35	-	-
	5.5	-	-	42.39	0.25	-	-
	7.5	-	-	33.74	0.16	-	-
	9.5	-	-	39.23	0.35	-	-
KNR 122	0.25	0.812	9.08 (± 2.21)	105.18	0.98	7.10	3.05
	0.75	0.767		112.51	0.73	13.32	3.58
	1.25	0.742	1.63 (± 0.49)	120.19	1.04	27.79	3.11
	1.75	0.742	-	124.67	0.86	25.64	3.03
	2.5	0.732	-	95.68	0.91	8.04	1.93
	3.5	0.722	-	95.46	0.87	9.53	1.95
	5.5	0.711	-	77.68	0.87	-	-
	7.5	0.672	-	85.67	0.91	-	-
	9.5	0.657	-	79.86	0.84	-	-
†KNR 130	0.25	0.833	12.96 (± 2.56)	218.77	5.66	2.90	1.41
	0.75	0.729	8.34 (± 2.12)	241.81	4.40	3.79	8.27
	1.25	0.737	3.28 (± 1.19)	251.23	2.40	11.29	6.48
	1.75	0.733	-	217.23	1.73	14.82	5.67
	2.5	0.706	-	177.96	1.35	17.64	5.29
	3.5	0.705	-	194.27	1.46	11.57	3.94
	5.5	0.707	-	148.20	1.27	32.64	3.22
	7.5	0.688	-	152.85	1.22	30.84	3.26
	9.5	0.680	-	153.05	1.16	22.53	2.95

Appendix cont.

Station	Avg. Depth (cm)	Porosity	Excess Th-234 (dpm g^{-1})	Fe concentration (umoles g^{-1})	Mn concentration (umoles g^{-1})	Pore water Fe (uM)	Pore water Mn (uM)
KNR 137	0.25	-	3.67 (± 0.42)	87.13	1.12	-	-
	0.75	-	2.29 (± 0.40)	96.19	0.97	-	-
	1.25	-	2.18 (± 0.36)	88.37	1.21	-	-
	1.75	-	-	107.33	1.55	-	-
	2.5	-	-	110.80	0.72	-	-
	3.5	-	-	111.30	0.43	-	-
	5.5	-	-	48.06	0.25	-	-
	7.5	-	-	38.30	0.18	-	-
	9.5	-	-	44.75	0.31	-	-
†KNR 140	0.25	0.701	6.70 (± 0.66)	102.57	1.71	6.75	25.93
	0.75	0.686	3.93 (± 0.52)	104.13	0.67	18.68	27.08
	1.25	0.662	1.65 (± 0.31)	114.35	0.84	8.12	17.09
	1.75	0.621	-	112.02	0.71	10.61	13.79
	2.5	0.596	-	116.20	0.80	12.17	9.52
	3.5	0.603	-	102.55	0.51	21.64	7.75
	5.5	0.548	-	93.72	0.56	21.39	5.79
	7.5	0.545	-	67.06	0.40	22.35	4.44
	9.5	0.528	-	52.59	0.35		
†KNR 147	0.25	0.901	22.67 (± 1.85)	319.72	2.17	4.41	5.57
	0.75	0.871	10.43 (± 0.75)	350.86	1.44	8.64	4.15
	1.25	0.857	2.32 (± 0.49)	306.35	1.24	8.06	2.85
	1.75	0.832	-	242.24	1.15	9.86	2.14
	2.5	0.824	-	193.82	1.04	14.04	1.87
	3.5	0.822	-	180.30	1.09	25.30	1.75
	5.5	0.817	-	154.43	0.93	24.33	1.53
	7.5	0.798	-	161.54	0.93	24.44	1.45
	9.5	0.819	-	191.83	0.93	20.28	1.42